Instituto de Astrofísica de Canarias

Trabajo Fin de Máster

Abundance of clustered Primordial Black Holes from Quasar Microlensing

Sven Heydenreich

supervised by
Evencio Mediavilla

January 21, 2018

Contents

1 Summary

1.1 English

Ever since its discovery, the nature of Dark Matter has been a subject of many studies, papers and projects. Despite nearly a century of research we are still unable to explain what forms about 80% of the matter in our Universe. While many believe that an unknown massive, collisionless elementary particle that only interacts gravitationally with baryonic matter is responsible for this phenomenon, there are some that argue that Dark Matter consists of MAssive Compact Halo Objects (MACHOs).

This hypothesis has received new attention following the results of the Laster Interferometer Gravitational Wave Observatory (LIGO). Since 2015, this observatory has reported the detection of 5 black-hole mergers (and one merger between neutron stars, containing an electromagnetic counterpart). The masses of those black holes exceeded the ones expected for stellar remnants, so that the discussion about primordial black holes received new input. These black holes formed shortly after the big bang out of quantum density fluctuations and are speculated to exist until today. They might be responsible for seeding the supermassive black holes in the centers of galaxies and are argued to be a reasonable candidate for dark matter: As they posess an enormous density they can be seen as nearly collisionless and, considering their mass, black holes are usually relatively dark. The masses and abundances of primordial black holes are constrained by Cosmic Microwave Background analysis, but there is a quite large mass range still open for these kinds of black holes.

One of the most useful tools to study Dark Matter is arguably gravitational lensing. This phenomenon is sensitive to the total matter, baryonic and dark, of the lensing object. In contrast to collisionless elementary particles, that form a smooth matter distribution and only significantly change over galactic distances, MACHOs can engage in microlensing, which is a peculiar form of gravitational lensing where the lensed object is not measurably displaced or distorted, but nonetheless immensely magnified. For this kind of gravitational lensing it is necessary that the source is extremely small. Usually, sources for gravitational microlensing are either stars or quasars (QUAsi StellAr Radio Sources). The unique aspect of microlensing is that it happens on small scales both spatially (light-day scales over cosmological distances) and timewise (ranging from several hours to months). This means that there are in general two kinds of study one can perform:

The first possibility is to observe objects over a long period of time and examine changes in flux, which can then be attributed to microlensing. The other possibility is to observe a large number of objects at one time and inspect the number of objects that are affected by microlensing. In both cases a statistical analysis needs to be performed afterwards. It seems evident that gravitational microlensing is an extremely helpful method to verify whether dark matter can exist of MACHOs.

In this thesis we will develop a method to probe the abundance of primordial black holes in lens galaxies using data of gravitationally lensed quasars. These extremely luminous objects are often lensed by other galaxies such that several images of the same quasar are visible, which allows us to determine the magnification due to microlensing of the images. We want to use data on several lensed quasars to determine this change in magnification and compare this with numerical simulations. To do this we will first develop an algorithm that constructs magnification maps for an arbitrary collection of microlenses. Afterwards we will write a script to extract the magnification histograms out of those maps and perform a bayesian analysis, using data from lensed quasars. We will discuss several uncertainties, especially the difficulty in determining the magnification of a lensed quasar.

This thesis builds on the work of Mediavilla et al. (2017), who already performed this analysis and concluded that the effect of primordial black holes would have been visible in microlensing data.

In addition to their work, we will consider an additional aspect: Due to the nature and formation of primordial black holes it is reasonable to assume that they primarily appear in clusters. We will therefore perform one analysis for a uniformly distributed set of microlenses and another one for a clustered set, comparing the results.

Apart from the fraction of mass in microlenses, which is the primary parameter in almost every gravitational microlensing experiment, we chose to parametrize the cluster radius and the number of black holes per cluster. Other possible parameters like the clustering efficiency or the source size had to be neglected due to finite processing power. We will discuss which values to choose for the seperate parameters and which effects the left-out ones could induce.

We find that, as expected, clustered black holes induce a slightly different magnification probability distribution and are in general less effective to cause microlensing (the mean values of the magnification maps differ by up to a factor of 2). Although we can not yet compare our analysis with real data due to limited processing power, we conclude that these differences might be enough to explain the apparent contradiction with current microlensing data. The reduced efficiency in microlensing might be the reason as to why we have not yet seen the effects of primordial black holes in quasar gravitational microlensing. However, determining the magnification of the real counterpart of the simulations is more difficult than in the case of a uniform distribution: The clusters of black holes appear for distant light rays as a single, massive lens which introduces huge caustics on the magnification maps that have a physical size which is larger than the broad line emission region and even spans a significant fraction of the narrow line emission region, both of which are usually used to determine a baseline for the magnification of the quasar as they are normally large enough that microlensing by single sources gets 'washed out'.

The code developed in this thesis will in the following weeks be used on a computer cluster to perform the analysis for a set of gravitationally lensed quasars and see whether the existence of clustered primordial black holes is consistent with current microlensing data.

1.2 Español

Desde su descubrimiento, la naturaleza de la Materia Oscura ha sido objeto de numerosos estudios, artículos cientificos y proyectos. A pesar de casi un siglo de investigaciones todavía somos incapaces de explicar lo que forma alrededor de 80 % de la materia en nuestro Universo. Mientras que muchos creen que una partícula elemental desconocida y masiva que sólo interactúa gravitacionalmente con la materia bariónica es responsable de este fenómeno, hay quienes argumentan que la Materia Oscura consiste principalmente en 'MAssive Compact Halo Objects' (MACHOs).

Esta teoría ha despertado nuevo interés tras los resultados del 'Laser Interferometer Gravitational-Wave Observatory' (LIGO). Desde 2015, este observatorio ha reportado la detección de 5 fusiones de agujeros negros (y una fusión entre estrellas de neutrones, detectándose la contrapartida electromagnetica). Las masas de estos agujeros negros han sobrepasado las esperadas para los restos estelares, alentado la discusión sobre los agujeros negros primordiales. Estos agujeros negros se formaron poco después del big bang de las fluctuaciones de densidad cuántica y se especula que siguen existiendo hoy en dia. Podrían ser las lemillas de los agujeros negros supermasivos que hay en los centros de las galaxias y son un candidato razonable para la materia oscura: Poseen una gran masa, no colosionan entre ello y son obscuros. Las masas y abundancias de los agujeros negros primordiales están restringidas por el análisis del fondo cósmico de microondas, pero todavía hay un rango de masas bastante grande, abierto para este tipo de agujeros negros.

Una de las herramientas más útiles para estudiar la materia oscura son las lentes gravitacionales.

El fenómeno lente gravitatoria es sensible a la materia total, bariónica y oscura, del objeto bajo estudio. A diferencia con las partículas elementales, que forman una distribución de la materia uniforme que sólo cambia significativamente sobre distancias galácticas, los MACHOs pueden actuar como microlentes, una forma peculiar de lentes gravitacionales donde el objeto óptico no se desplaza o distorsiona mensurablemente, pero sin embargo se magnifica intensamente. Para que este tipo de lentes gravitacionales, es necesario que la fuente sea pequeña. Por lo general, las fuentes de microlente gravitacional son estrellas o cuásares (QUAsi StellAr Radio Sources). Un aspecto único del efecto microlente es que ocurre a pequeña escala tanto espacialmente (escalas de día-luz sobre distancias cosmológicas) como cronológicamente (entre varias horas y meses). Esto significa que en general hay dos tipos de estudios que se pueden realizar.

La primera posibilidad es observar los objetos durante un período de tiempo largo y examinar los cambios en el flujo, que pueden atribuirse al efecto microlente. La otra posibilidad es observar una sola vez un gran número de objetos y estudiar el impacto del efecto microlente. En ambos casos es necesario realizar posteriormente un análisis estadístico. Estudios previos demuestran que el efecto microlente es un método extremadamente útil para investigar si puede existir materia oscura en forma de MACHOs.

En esta tesis desarrollaremos un método para estimar la abundancia de agujeros negros primordiales en galaxias lentes usando datos de cuásares en sístemas lente. En estos sístemas, varias imágenes del mismo cuásar son visibles, lo que nos permite determinar la magnificación debída al efecto microlente. Queremos utilizar los datos de varios sístemas lente de quásares para determinar este cambio en la magnificación y compararlo con simulaciones numéricas. Para ello, primero desarrollaremos un algoritmo que construye mapas de magnificación para una colección arbitraria de microlentes. Después escribiremos un código para extraer los histogramas de magnificación de esos mapas y realizar un análisis Bayesiano, usando datos observacionales de cuasares en sístemas lente. Discutiremos varias tuentes de incertidumbre, especialmente la dificultad para determinar la magnificación de un cuásar en un sístema lente.

Esta trabajo fin de máster se se basa en el estudio de Mediavilla et al. (2017), quien ya realizó este análisis y concluyó que el efecto de los agujeros negros primordiales habría sido visible en los datos de microlensing. Para amlíar este trabajo, consideraremos un aspecto adicional: debido a la naturaleza y formación de los agujeros negros primordiales es razonable suponer que aparecen principalmente en cúmulos. Por lo tanto, realizaremos un análisis para un conjunto de microlentes uniformemente distribuido y otro para un conjunto agrupado encúmulos, comparando los resultados.

Aparte de la fracción de masa en microlentes, que es el parámetro principal en casi todos los estudios de microlentes gravitacionales, elegiremos como otros parámetros libres el radio del cúmulo y el número de agujeros negros por cúmulo. Otros posibles parámetros como la eficiencia del 'clustering' o el tamaño de la fuente tuvieron que ser omitidos debido a la potencia de procesamiento finita. Discutiremos qué valores elegir para estos parámetros.

Encontramos que, como era de esperar, los agujeros negros agrupados encúmulos inducen una distribución ligeramente diferente de la probabilidad de magnificación y, en general, son menos efectivos (los valores medios de los mapas de magnificación difieren hasta en un factor 2). Aunque aún no podemos comparar nuestro análisis con los datos reales debido a la limitada capacidad de procesamiento, concluimos que estas diferencias podrían explicar o reducir la aparente contradicción con los datos de microlensing actuales encontrada por (Mediavilla et al. 2017). La reducción en la eficiencia del efecto microlente podría ser la razón por la cual aún no hemos visto los efectos de los agujeros negros primordiales en los sistemas múltiples de cuásares. Sin embargo, determinar la magnificación de las simulaciones es más difícil que en el caso de una distribución uniforme: Los

cúmulos de agujeros negros se comportan (para los rayos de luz distantes) como una sola lente masiva que introduce enormes cáusticas en los mapas de magnificación. Estas cáusticas gigantes tienen un tamaño físico que es más grande que la región de emisión de líneas anchas e incluso una fracción significativa de la región de emisión de líneas estrechas. Estas regiones se usan, habitualmente, para determinar el estado de no 'microlensing', respecto del cual se mide la magnification inducida por este efecto. Esta función podira verse afectuda por la puesencia de las cáusticas giganes.

El código desarrollado en esta tesis se utilizará en las próximas semanas en un clúster de ordenadores para realizar el análisis de los datos reales un conjunto de cuásares en sístemas lente para ver si la existencia de agujeros negros primordiales agrupados en cúmulos es consistente con las observaciones actuales.

2 Introduction, Motivation and Objective

It is not hard to believe that since humankind became sentient, we have looked up to the stars and wondered what they are, what they mean and what our place in the Universe might be. In fact, detailed observations of stellar constellations, comets and even supernovae can be traced back several millenia. But although the branch of astronomy is extremely old, we have just recently discovered technological means to significantly improve the quality of our observations. One of the most impactful discoveries of recent times was made by Zwicky (1933): Observing spectroscopic images of galaxy clusters he found out that the kinetic energy of the single galaxies is by far too large for the cluster to be a gravitationally bound structure. On the other hand, the crossing timescale of a galaxy cluster is less than the Hubble time, which makes the assumption that galaxy clusters are gravitationally bound highly likely. Zwicky concluded that something invisible has to be inside the clusters, keeping them together – and Dark Matter was born. Despite nearly a century of research and the development of far more advanced tools (as for example digital tracking systems and CCD chips) we are still unable to understand and explain the nature of this phenomenon.

In modern Astrophysics, Dark Matter is needed to explain a variety of phenomena ranging from large scales (galaxy clusters, cosmic web) to intermediate ones (dynamics of galaxies). This distracts from the fact that Dark Matter is just a name for a phenomenon we can not yet explain. While some argue that the underlying phenomenon is a modified theory of gravity, the more popular opinion is that it is a collisionless form of matter that can only interact gravitationally with baryonic matter. The favoured hypothesis is that Dark Matter consists of a still unknown elementary particle, however even at the Large Hadron Collider no direct evidence for such a particle has been found (one experiment that might change that is the DAMPE-satellite (DAMPE Collaboration et al. 2017)). This fueled the hypothesis that Dark Matter consists of MAssive Compact Halo Objects (MACHOs), especially black holes. As black holes can also be considered invisible and collisionless, they pose a reasonable candidate for Dark Matter. However a microlensing survey of the Small and Large Magellanic Clouds yielded no conclusive result (Becker et al. 1999). Additionally to that, these MACHOs must be of primordial nature (meaning that they formed very shortly after the big bang, way before the time of recombination), as the fraction of baryons in our universe is well constrained by the results of the Planck mission (Planck Collaboration et al. 2016). Due to this and the fact that, under most formation models, those primordial black holes must have left a visible imprint in the cosmic microwave background (Poulin et al. 2017), MACHOs did not seem to be an interesting candidate to compose dark matter. However, they were never completely ruled out as a potential candidate and many models of primary black hole formation are consistent with current CMB analysis results (Nakama et al. 2017; Ezquiaga et al. 2017).

The debate has recently received new input by the LIGO-collaboration and their direct detection of gravitational waves (Carr et al. 2016). An analysis of their results yielded the masses of the colliding black holes: $36M_\odot$ and $29M_\odot$, $14M_\odot$ and $7.5M_\odot$, $31M_\odot$ and $19M_\odot$, $31M_\odot$ and $25M_\odot$, $12M_\odot$ and $7M_\odot$ (Abbott et al. 2017a, 2016a, 2017c, 2016b, 2017b). Those merging black holes might just be stellar remnants, although their masses appear to be unusually high (Elbert et al. 2018; Cao et al. 2018). However they lie in a mass range which is not excluded as a potential PBH mass range by CMB analysis (Ezquiaga et al. 2017). This might be a big coincidence, the gravitational lensing of gravitational waves (Dai et al. 2017; Smith et al. 2017) or an unknown selection bias, but another reasonable explanation might be the existence of primordial black holes composing dark matter (García-Bellido 2017; Clesse & García-Bellido 2017b,a).

Mediavilla et al. (2017) suggested to determine constraints on the abundance of compact lensing objects using microlensing magnifications of gravitationally lensed quasars. In contrast to previous microlensing studies, a wider mass range exceeding stellar values was considered, still the results are consistent with the assumed stellar population. However, in this thesis we will consider that the lensing black holes are likely to be clustered, which might pose different results than uniformly distributed lenses (García-Bellido & Clesse 2017).

The objective of this thesis is thus to analyse the microlensing capabilities of clustered microlenses, compared to those of uniformly distributed lenses. We want to see whether the existence of clustered primordial black holes is consistent with quasar microlensing data, which is not the case for uniformly distributed primordial black holes (Mediavilla et al. 2017). To do this, we will develop a python code to create numerical simulations of gravitationally microlensed quasars (see Section 3.2). After that we will use another program to perform a bayesian analysis on these simulations (compare Section 3.6). We will apply this procedure to some representative examples in Sections 4.3 and 4.4.

In the end the program should be used on a computer cluster to perform the simulations for a sample of gravitationally lensed quasars, which then will be analysed in a Bayesian way. Due to the huge amount of calculations needed this will not be a part of the thesis.

The reader of this thesis should know the basics of cosmology. A brief summary of gravitational lensing, focusing on microlensing, will be given in Section 3.1.

3 Methodology and Calculations

3.1 Gravitational Lensing

At first, a brief introduction on gravitational lensing, introducing the most important quantities, will be given. This section heavily relies on Schneider (2015); Meylan et al. (2006). In the framework of general relativity, photons, as any other objects that are not subject to external forces, move along geodesics in the four-dimensional spacetime manifold. Contrary to a baryonic observer, for photons the proper time $\tau = c\,ds$ is zero. In practical contexts the gravitational potential Φ can mostly be regarded as small, meaning $\Phi/c^2 \ll 1$, which is satisfied everywhere except in the immediate vicinity of neutron stars or black holes. This means that one can linearize the Einstein Field Equations, giving rise to a way easier mathematical framework.

As in a gravitational lensing event both the extent of the source and of the lens are neglible compared to the distances involved, one usually speaks of a *Source Plane* and a *Lens Plane*. The main advantage is that we can define the *Surface Mass Density* Σ for a two-dimensional coordinate

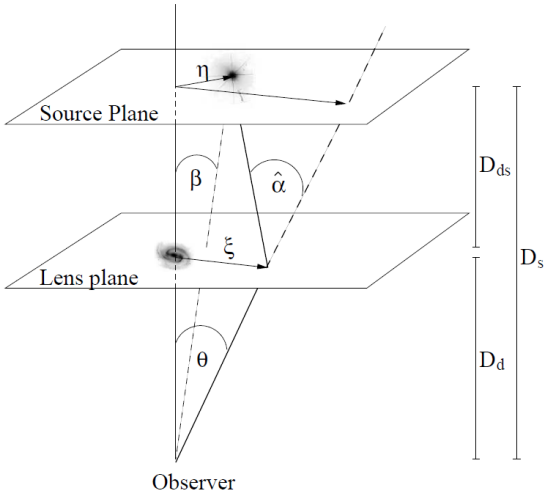

Figure 1: The Geometry of a Gravitational Lensing Event (Schneider 2015).

$\boldsymbol{\xi}$ as the line-of-sight integral

$$\Sigma(\boldsymbol{\xi}) = \int \mathrm{d}z\, \rho(\boldsymbol{\xi}, z) \ ,$$

where ρ is the normal matter density. This consideration lets us handle every[1] problem in gravitational lensing as a two-dimensional one. The geometry of a gravitational lensing event can be depicted in Figure 1. Here, D_d is the (angular diameter) distance[2] between observer and lens, D_s is the distance between observer and source and D_ds constitutes the distance between lens and source. One might be tempted to set $D_\mathrm{ds} = D_\mathrm{s} - D_\mathrm{d}$, but this is not true for extragalactic distances due to the nonlinearity of the Hubble flow. The parameter $\boldsymbol{\theta}$ describes the apparent position of the source in the sky, whereas $\boldsymbol{\beta}$ describes its true position. $\boldsymbol{\xi} = D_\mathrm{d}\boldsymbol{\theta}$ and $\boldsymbol{\eta} = D_\mathrm{s}\boldsymbol{\beta}$ are the corresponding projected distances and $\hat{\boldsymbol{\alpha}}$ is the deflection angle, which can be calculated by the field-equations of general relativity. For a point mass, this deflection angle reads $\hat{\boldsymbol{\alpha}} = \frac{4GM}{c^2\xi^2}$. In linear order, we can achieve a formula for a general mass distribution by superposition. If we define the scaled deflection angle $\boldsymbol{\alpha}$ via the lens equation

$$\boldsymbol{\beta} = \boldsymbol{\theta} - \boldsymbol{\alpha}(\boldsymbol{\theta}) \ ,$$

simple geometry dictates

$$\boldsymbol{\eta} = \frac{D_\mathrm{s}}{D_\mathrm{d}}\boldsymbol{\xi} - D_\mathrm{ds}\hat{\boldsymbol{\alpha}}(\boldsymbol{\xi})$$

and by integration we get a lens equation for a general mass distribution:

$$\boldsymbol{\alpha}(\boldsymbol{\theta}) = \frac{1}{\pi}\int d^2\theta' \kappa(\boldsymbol{\theta}')\frac{\boldsymbol{\theta} - \boldsymbol{\theta}'}{|\boldsymbol{\theta} - \boldsymbol{\theta}'|^2} \ . \tag{1}$$

[1] Except the calculations involved in the analysis of cosmic shear.
[2] It should be noted that all distances in gravitational lensing are angular diameter distances.

Here the convergence κ is defined as

$$\kappa(\boldsymbol{\theta}) = \frac{4\pi G D_\mathrm{d} D_\mathrm{ds}}{D_\mathrm{s} c^2} \Sigma(D_\mathrm{d}\boldsymbol{\theta}) =: \frac{\Sigma(D_\mathrm{d}\boldsymbol{\theta})}{\Sigma_\mathrm{cr}} \,. \tag{2}$$

If one imagines a point-source, a compact lens and a perfect alignment of observer - lens - source, symmetry dictates that the source should appear as a ring-like structure around the lens. The radius of this ring is a characteristic quantity, called the *Einstein Radius*

$$\theta_\mathrm{E} = \sqrt{\frac{4GM}{c^2} \frac{D_\mathrm{ds}}{D_\mathrm{d} D_\mathrm{s}}} \,. \tag{3}$$

The Einstein Radius is usually projected onto the source plane my multiplying with the angular diameter distance D_s.

Apart from the obvious change in position it is interesting to observe a change in the size of an object. This change can be characterized by the matrix

$$A = \frac{\partial \boldsymbol{\beta}}{\partial \boldsymbol{\theta}} \tag{4}$$

where $\mu = \det(A)^{-1}$ is the magnification at one coordinate.[3] The magnification matrix can be written in the following form (Meylan et al. 2006):

$$A = \begin{pmatrix} 1-\kappa-\gamma_1 & -\gamma_2 \\ -\gamma_2 & 1-\kappa+\gamma_1 \end{pmatrix} \,,$$

where $\boldsymbol{\gamma} = (\gamma_1, \gamma_2)$ is the twodimensional *shear*. This quantity is especially important in the study of weak gravitational lensing, whereas here we are just interested in its absolute quantity $\gamma = |\boldsymbol{\gamma}|$. Calculating the determinant we find that the magnification in a point becomes

$$\mu = \frac{1}{|(1-\kappa-\gamma)(1-\kappa+\gamma)|} \,. \tag{5}$$

Small objects like stars, planets or stellar remnants normally can not produce any detectable displacement of sources, however they can significantly magnify sources. The study of these magnifications falls under gravitational microlensing and is an exceptionally interesting subject, as it is one of the only cosmological phenomena that are not stationary over human timescales.

Usually, microlensing is performed by compact objects which we can safely approximate as point-masses. Scaling $\boldsymbol{x} = \boldsymbol{\theta}/\theta_\mathrm{E}$ and $\boldsymbol{y} = \boldsymbol{\beta}/\theta_\mathrm{E}$, the lens-equation for a point-mass becomes

$$\boldsymbol{y} = \boldsymbol{x} - \frac{\boldsymbol{x}}{|\boldsymbol{x}|^2} \,.$$

For a single point-mass lens one can find an analytical solution for the magnifications, however for two or more lenses those are impossible to find (Meylan et al. 2006). The main reason for this is that in the case of a more complicated lens system, multiple images of the same source can exist.[4]

[3] It should be noted that the surface brightness of an object never changes, only its angular extent. For point-like sources like stars and quasars however, this corresponds to a direct increase in observed brightness.

[4] Technically this is also the case for a point-mass lens, but for all physical applications the second image is behind the lens, so that it is not observable.

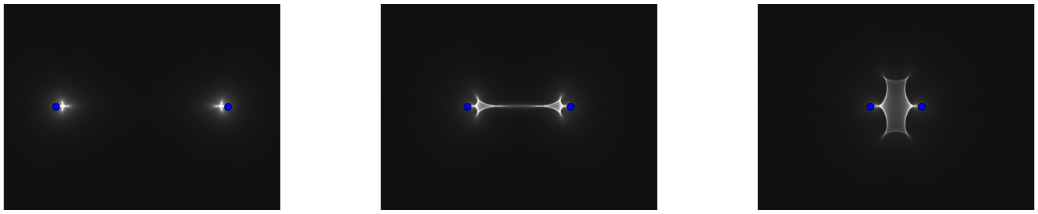

Figure 2: Caustic pattern for a binary lens of different separations. The blue circles depict the lenses.

If we imagine a source far away from the lens, then this source has one image as it is only weakly distorted by the lens. However, when we move the source closer to the lens there has to be a point where an additional image is created. This point lies on a curve called *caustic* (in the source plane) or *critical curve* (in the lens plane). Whenever a source 'crosses' such a caustic, an image pair gets either created or destroyed. One might think that this is a peculiar phenomenon: We are given a function $\boldsymbol{\beta}(\boldsymbol{\theta})$ with a differential A, so we can simply use the inverse function theorem, construct a function $\boldsymbol{\theta}(\boldsymbol{\beta})$ and the creation of image pairs should be impossible. One aspect prohibits us from doing that: On these caustics the magnification μ diverges, which means that the determinant $\det(A)$ vanishes. This permits us from creating an inverse function in these regions and is the reason why analytical solutions for problems in gravitational lensing are extremely rare.

A sample of binary lenses and their respective caustics is depicted in Figure 2. As one can see, if the lenses are far apart from each other, the point-like singularity deforms into a little asterisk. When the lenses move closer to each other these asterisks get bigger and start to merge. Finally, for close lenses the caustics form a single, big asterisk.

In this thesis we will analyze gravitational lensing by black holes scattered in a galaxy, or, in other words, lensing by compact objects in a smooth background gravitational field. For this we use the *Chang-Refsdal lens* equation (Chang & Refsdal 1979):

$$\boldsymbol{y} = \begin{pmatrix} \kappa_s + \gamma & 0 \\ 0 & \kappa_s - \gamma \end{pmatrix} \boldsymbol{x} + \sum_i m_i \frac{\boldsymbol{x} - \boldsymbol{x}_i}{|\boldsymbol{x} - \boldsymbol{x}_i|^2} \,. \tag{6}$$

Here, γ represents the shear introduced by the galaxy whereas κ_s is the convergence in smooth matter and the m_i and $\boldsymbol{x}_i$ represent the masses[5] and positions of the single microlenses. As the lens-equation is linear, we can simply summarize the deflections caused by the smooth matter and the different compact lenses.

3.2 Obtaining Magnification Maps

The objective of this thesis is to perform a microlensing analysis on gravitationally lensed quasars. To model a microlensing event, one has to compute a *Magnification Map*. This means one has to construct a gravitational lens and compute the magnification pattern that arises in the source plane, which allows us to estimate the probability of a given magnification of the source.

As discussed in the previous section, the magnification $\mu = \det(A)^{-1}$ is theoretically easy to obtain. Unfortunately it is impossible to find a function that maps each point on the source plane

[5]The masses in this equation are unitless, they are scaled by the mass chosen in the Einstein Radius.

to the corresponding point on the lens plane. The mathematical reason for that is the vanishing determinant of A, but a more intuitive approach might be this:

We know that the number of images that a source has on the lens plane depends on its position, i.e. there are sources that have only one images and sources with several images. This means that we need to assign a different number of images to different points, which a function can not do. Additionally, a source with five images, that can not be resolved by a telescope, will appear as bright as the sum of all the five image fluxes. All things considered, we find that it is impossible to construct an analytical function to assign a magnification to a point in the source plane. We thus have to rely on a more brute-force method.

3.2.1 Inverse Ray Shooting

The easiest way to compute magnification maps is the so-called Inverse Ray Shooting (IRS) algorithm (Schneider & Weiss 1987b). In this process, we use the fact that light-rays are invariant under time-reversal. This means that instead of trying to construct an inverse function to the lens equation we imagine a photon sent out from the observer that then gets deflected by the lens and arrives at a coordinate of the source plane. As gravitational lensing does not change surface brightness, the magnification at a point of the source plane is directly proportional to the amount of rays that hit this point.

In our python script we choose a twodimensional grid (an empty array of size N_y) as the Source Plane. We then shoot a certain number N_r of light-rays per unit area. Assuming a given κ, γ and a distribution of microlenses N_*, each 'light-ray' gets deflected by the lens-equation (6) and (sometimes) reaches a certain pixel on the source-plane. The value of this pixel then gets raised by one. In the end the array is normalized by the amount of rays that would hit each pixel in absence of lensing.

An important aspect is the size of the shooting region. We want the region to be big enough to contain most of the rays that finally hit the source plane, but not too big to avoid unnecessary computations. Especially, due to shear, the shooting region is not quadratic, but rectangular. In general, one axis of the shooting region is taken to be $x_{l,1} = 1.5 * N_y/|(1-\kappa-\gamma)|$ and the other axis is $x_{l,2} = 1.5 * N_y/|(1-\kappa+\gamma)|$. The denominators account for the magnification in the respective axes (compare (6)) whereas the factor 1.5 ensures that enough rays hit the boundary regions.

Now one has to think about distributing an appropriate amount of microlenses. For this the parameter α, the *fraction of mass in microlenses* is essential. From this one can calculate the convergence in microlenses $\kappa_* = \alpha\kappa$ and the smooth convergence $\kappa_s = \kappa - \kappa_*$. From the definition of convergence we can conclude that for a square region of size L (again in Einstein radii) one would need

$$N_* = \kappa_* L^2/\pi \tag{7}$$

microlenses. However, there is another issue that we need to consider:

Due to the fact that close encounters of microlenses may deflect lightrays significantly it is highly likely that some of the lightrays that would originally hit the source plane instead miss it. On the other hand it is also almost certain that some lightrays might hit our source plane due to deflectors residing outside of the region where the stars are distributed. To consider all but a small fraction ϵ (in our case we set $\epsilon = 0.02$) of this *diffuse flux*, the number of stars needs to be at least (Schneider & Weiss 1987a)

$$N_* = \frac{3\kappa_*^2\epsilon^{-1}}{(1-\kappa)^2-\gamma^2} ,$$

from which we can, using (7), calculate a minimum size of the deflector region $L_{\min}$. The size of the deflector region is then

$$L = L_{\min} + 2\max(x_{l,1}, x_{l,2}) \ .$$

Inserting this in (7) we finally get the number of needed microlenses, that we can distribute in a region of size L however we see fit. Normally a uniform distribution is preferred, but in our thesis we will handle this process differently.

In Mediavilla et al. (2016) an example code is given. At first we replicated the code and started performing some optimizations: As each row of rays is independent of the others, it is possible to spawn n independent processes that each shoot every n-th row of rays and collect the result in their seperate array.[6] These arrays get, in the end, passed to a queue and the processes get terminated. Upon adding the arrays an increase in performance of the factor 2-16 (depending on the number of cores on the CPU) is achieved.

However an important issue of this method is still computing time. For each ray shot the deflection is calculated for each lens, which leads to an amount of

$$\frac{N_y^2 N_\mathrm{r} N_*}{|(1-\kappa-\gamma)(1-\kappa+\gamma)|}$$

calculations needed. To achieve good statistics (especially in the low-magnification regions where not so many rays hit a pixel) a number of $N_\mathrm{r} \gg 100$ is needed. For our needs, values of $N_y = 1000$, $\kappa \approx \gamma \approx 0.45$ and $N_* \gtrsim 10\,000$ are reasonable and we would need more than 10^{14} calculations. Unfortunately even with our optimizations the calculation of a single viable map would take several days. Fortunately, there are ways to improve on the inverse ray-shooting method.

3.2.2 Inverse Polygon Mapping

The main problem with the inverse ray shooting algorithm is its noise in low-magnification regions. Each light-ray represents a unit area that gets mapped on the grid of the source plane. If such a unit area is spread out over several pixels, still only the value of the pixel containing its center is raised, all others are not affected. To ensure proper statistics, a huge number of rays per pixel is necessary. The *Inverse Polygon Mapping* (IPM) algorithm (Mediavilla et al. 2011, 2006) improves on this method, cutting the computational time by a factor of the order of 100.

As in the IRS algorithm, we shoot a uniform grid of rays that again gets deflected by the lens equation. Now, instead of simply raising the pixel values by one, we consider the image of each *square* of the ray-shooting grid. Due to a symmetry in the lens equation (Meylan et al. 2006), to first order those squares are mapped to parallelograms, so we can interpolate a parallelogram between the images of the four vertices. Then, as proven by Mediavilla et al. (2006), if the intersecting area of a pixel and such a parallelogram is $\Delta\boldsymbol{S}'$, then the pixel has collected $\Delta\boldsymbol{S} = \Delta\boldsymbol{S}'/\det(A)$ light of the image plane, where A is the magnification matrix (4) which can, to linear order, be calculated from the images of the vertices. The intersecting area can be computed using Green's theorem, which states that for a surface $\boldsymbol{S}$ with oriented, simple boundary C its area corresponds to the integral

$$\int_C -y_2 \,\mathrm{d}y_1 \ .$$

[6] The rays are always shot row-wise as python handles arrays much faster than for-loops.

A good intuitive comparison between inverse ray shooting and this method would be that IRS corresponds to a zeroth-order taylor approximation and this method corresponds to a first-order one. Still, one problem arises: If the square is crossed by a critical curve, the boundary curve is not necessarily oriented and simple. These cells need to be treated specially, either by breaking them down into smaller, regular cells or by treating these cells with an IRS algorithm.[7]

If instead of a square lattice one shoots square-centered cells, the additional information of the center of the cell suffices (again due to symmetry in the lens-equation) to solve the second-order taylor expansion of the lens-equation. In addition to a better representation of the mapped cells it also gets easier to identify nonlinear regions (corresponding to cells on critical curves).

This process needs a considerable amount of calculation (instead of just raising the value of an array by one), so with the same number of rays per unlensed pixel such an algorithm takes about three times longer. However, the noise of an IPM algorithm is so much lower, that one can receive better results with a value of about 0.12 rays per pixel than an IRS algorithm with 500 rays per pixel. All things considered, the IPM algorithm offers a cut of a factor of 100 in computational time while still offering better statistics.

Unfortunately, the construction of such an algorithm would go beyond the scope of the thesis, so that we used one supplied by Mediavilla et al. (2011) and only modified it to fit to our needs.

3.3 Clustered Primordial Black Holes

As already discussed, in this thesis we want to consider clustered black holes microlensing a background quasar. If primordial black holes in the mass range of the LIGO-detections do indeed exist, they should leave a visible imprint due to their gravitational microlensing effects. Mediavilla et al. (2017) have discussed the possible effects in the field of quasar gravitational microlensing and concluded that the existence of PBHs is unlikely. In this thesis we will assume that those black holes are likely to be clustered, which might significantly change their microlensing properties. The assumption of a clustering of PBHs is justified: They originated due to density fluctuations shortly after the big bang. At a point where the density is high and a PBH forms, there are likely other points nearby that also allow for the formation of a PBH (compare Figure 3).[8]

For our IPM program, we need to construct a *stars.dat* file, containing positions and masses of all considered microlenses. García-Bellido & Clesse (2017) analyzed the possible properties of clustered primordial black holes taking into account results from LIGO, gravitational lensing and CMB analysis. They assumed a lognormal distribution of black-hole masses centered around $\sim 25 M_\odot$ (Ezquiaga et al. 2017) and concluded that while the number of black holes per cluster at formation was of the order of 2000, due to dynamical friction and mergers the number today should be around 100 to 1000. Additionally they concluded that when the clusters extent is on sub-parsec scales, then the existence of clustered primordial black holes is consistent with CMB restrictions.

In this thesis we will consider black holes of constant mass, as gravitational microlensing is not very sensitive to the slope of the mass spectrum but rater to the average mass (Congdon et al. 2007). The algorithm itself is unitless, so that we do not have to specify an average mass yet. Moreover, the translation to physical values is via the Einstein radius (3), so to scale between different masses one simply has to divide by the square root of their ratio. Whenever we use physical values, unless

[7] As critical curves are mapped onto caustics, which occur only in high magnification areas, the high noise of the IRS algorithm in low magnification areas is insignificant.

[8] This Figure is not entirely correct as the limit for the collapse into a black hole is not only dependent on density but also on the size of the region. However, it should serve to give a reasonably good understanding.

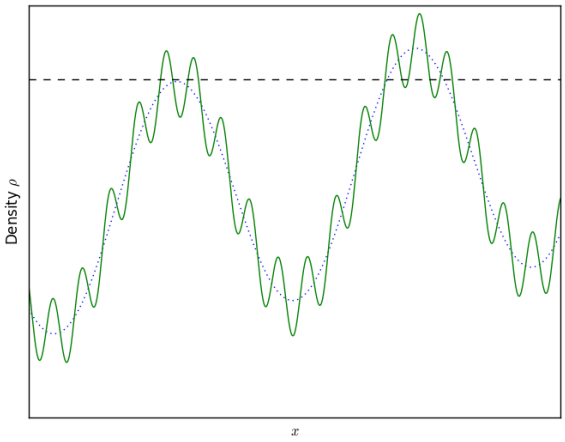

Figure 3: A two-mode density fluctuation (green line) with an artificial density limit (black line) imposing the collapse to a black hole.

otherwise specified, we will assume a black hole mass $m_{\mathrm{BH}} = 30\mathrm{M}_{\odot}$, a lens redshift of $z_{\mathrm{L}} = 0.5$ and a source redshift of $z_{\mathrm{S}} = 2.0$.[9] Considering Mosquera & Kochanek (2011), those seem to be quite typical values.

Regarding the radial profile of the clusters one might be tempted to use a Navarro-Frenk-White profile, as they are omnipresent when cold dark matter is considered (Navarro et al. 1996, 1997). However, the equation rather describes the global structure of dark matter in a galaxy or a galaxy cluster and is not supposed to be used on parsec-scales. As we have no prior knowledge about the radial profile of clusters of black holes and we believe that among the many systematic uncertainties this one is quite neglible we chose to apply a Gaussian radial profile with deviation σ.

3.4 Source Size Effects

Even to the best telescope every quasar looks like a point-source. However, while in microlensing the Einstein radii of stars and black holes are still larger than the (continuum) source size by one or two orders of magnitude (Mosquera & Kochanek 2011), the caustic patterns sometimes have a much smaller extent, so that the source size plays a significant role in the magnification. If, for example, a quasar has a twodimensional profile $F(\boldsymbol{x})$ and the magnification map is a function $\mu(\boldsymbol{x})$ then the total magnification of the quasar μ_{Q} at point $\boldsymbol{x}_0$ reads:

$$\mu_{\mathrm{Q}}(\boldsymbol{x}_0) = \sum_{\boldsymbol{x}} F(\boldsymbol{x}_0 - \boldsymbol{x}) * \mu(\boldsymbol{x}) \ ,$$

so it is a *convolution* between the source profile and the magnification map. However, while the source size is extremely important, microlensing is less sensitive to the radial profile of the source

[9] For the calculation of the angular diameter distances we will assume a flat universe with $H_0 = 70\mathrm{km\,s^{-1}\,Mpc^{-1}}$, $\Omega_{\mathrm{M}} = 0.3$ and $\Omega_{\Lambda} = 0.7$.

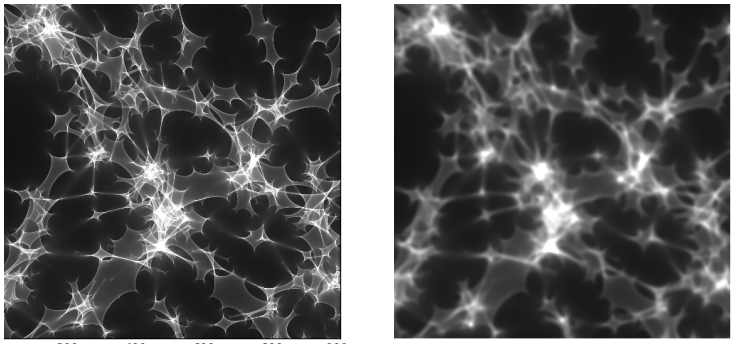

(a) Unconvolved Map (b) Convolved Map (5px)

(c) Convolved Map (10px) (d) Convolved Map (20px)

Figure 4: Magnification Map of 1000 pixels convolved with a gaussian with deviation of 5, 10 and 20 pixels.

(Mortonson et al. 2005). Due to this fact, it is easiest to convolve the resulting magnification map with a twodimensional gaussian. This leads to a 'blurring' of the magnification map, where the high-magnification regions (i.e. caustics) get washed out (compare Figure 4). This effect is also clearly apparent when one considers a histogram of the magnifications. Spikes in the histogram get smoothed and the appearance changes significantly (compare Figure 5).

3.5 Determining the Magnification

While in our simulations the determination of the magnification is completely straightforward, measuring the magnification of an observed quasar is surprisingly difficult. The intrinsic luminosity of the quasar is unknown and one has to separate magnification by microlensing from the global magnification and the intrinsic variability of the quasar itself. Additionally, effects like extinction due to dust can play a significant role. Considering these effects, the determination of magnification due to microlensing of a single image is impossible, one instead has to compare different images of the same quasar. Mediavilla et al. (2009) present a good overview on how to approach this.

At first, it is important to construct a *baseline* describing the observed luminosity of a quasar in absence of microlensing. Usually, the narrow line emission region and, to some extent, the broad-

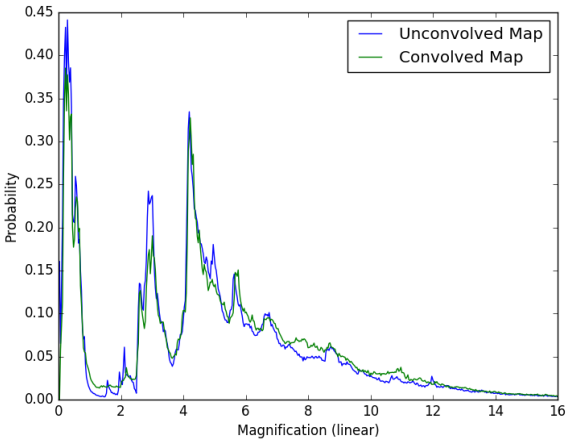

Figure 5: Magnification Histogram of a Map before and after convolution with a gaussian source.

line emission region are large enough that the effects from microlensing get 'washed out' (Mosquera & Kochanek 2011; Chen et al. 2011; Yonehara 2006; Bennert et al. 2002). The continuum emission region however, measuring only about 5 lightdays (Fausnaugh et al. 2016; Mediavilla et al. 2009), is very sensitive to microlensing. If one analyzes multiply imaged quasars, then from the flux-ratio of their emission line regions one can determine the difference in magnification due to the galaxy. Then, considering the continuum emission data, one can calculate a magnification difference in microlensing. In some cases the radio emission can also be used as a baseline, however radio emission passes through dust differently, so possible extinction effects might go unnoticed. In the most desperate case it is also possible to construct a global lens model using the astrometry of the quasars, but it is completely impossible to account for extinction effects and naturally it is highly model-dependent.

In our case we face another problem. Looking at Figure 6 it is apparent that in addition to the caustic structure caused by the single black holes (which is barely visible) there is another structure superimposed: The caustics caused by the clusters. If the light ray passes outside of the cluster it acts like a microlens with a mass of all black holes combined, causing immense caustics. In this image, which is 1000×1000 pixels, one pixel corresponds to approximately 5 lightdays and one can see that some structures easily span the whole map, corresponding to several parsecs. This *millilensing* surpasses the broad line emission region by at least an order of magnitude, which means that this region will be completely useless in determining the baseline. We will have to investigate whether we could still use the narrow line emission region, but mostly we will probably have to consider the quasars radio emission.

3.6 Statistical Analysis

The final goal of the numerical simulation is to compare the results with real observations. Let the images A and B of a quasar have a difference in magnitudes of Δm. From the constructed magnification maps we can extract for each set of parameters α_i magnification histograms $H_A(m, \alpha_i)$ and $H_B(m, \alpha_i)$ that assign a probability to each magnification m, for each image respectively. The

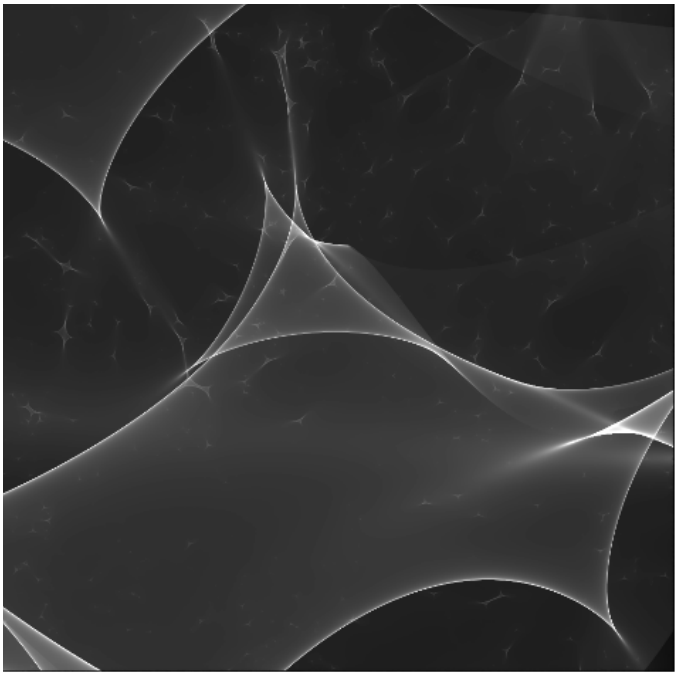

Figure 6: Magnification Map produced by clustered black holes.

probability of observing a certain magnitude difference Δm can be written as

$$P(\Delta m|\alpha_i) = P(m_B - m_A = \Delta m|\alpha_i) = \int \mathrm{d}m\, H_B(\Delta m + m, \alpha_i) H_A(m, \alpha_i) \;, \tag{8}$$

which is a crosscorrelation of the histograms. After that we can use Bayes Theorem, which states that the likelihood of a set of parameters reflecting the model, given a measurement, is proportional to the probability of getting this measurement in the model, given the parameters:

$$L(\alpha_i|\Delta m) \propto P(\Delta m|\alpha_i) \;.$$

This means that after extracting the histograms, we simply have to convolve the appropriate ones for each choice of parameters, normalize the resulting histogram and consider the probability of the bin reflecting the actual measurement. Finally we plot the probabilities respective to the parameters. Special care needs to be taken with the normalisation of the histograms, as an unequal normalisation would completely ruin the analysis. The set of parameters that we do not want to consider gets marginalized.

It is the usual procedure to perform such a bayesian analysis on a huge sample of quasars, instead of performing it on just one object. In this case the final likelihood distributions for each of the quasars get multiplied, with the final likelihood distribution being the resulting product.

Table 1: Values chosen for the computation of magnification maps.

Parameter	Values
α	0.1, 0.2, 0.3, 0.4, 0.5, 0.6, 0.7, 0.8, 0.9 and 1.0
N_{BH}	100, 300 and 1000
σ	2, 4 and 10

4 Results

4.1 First Considerations

The main limit to this analysis is computational power. As we want to observe phenomena that happen on quite large scales (compared to other microlensing events), the maps need to have a large size. Unfortunately, an increase in size does not only increase the number of rays that need to be shot but also in the same way the number of microlenses. If one doubles the map size, one should expect the computational time to increase by a factor of 2^4. Due to this reason we chose to model relatively small maps (with an extent of 40 Einstein radii). To obtain statistically significant results we chose to compute 100 maps for each choice of parameters. As the main parameters, as discussed in Section 3.3, we chose the fraction of mass in microlenses α (which is our main interest), the number of black holes per cluster N_{BH} and the extent of the cluster σ (in Einstein radii). The values chosen can be seen in Table 1. Due to lack of computational power we were unable to consider other variables like source size, radial cluster profile, clustering of clusters or clustering efficiency (i.e. the fraction of *loose* black holes that not belong to a cluster). Also, one important aspect is that we could not consider is the population of stars present in the galaxy: As we are dealing already with up to 50 000 microlenses per image, adding a population of stars, whose mass is two orders of magnitude lower, would skyrocket our number of microlenses to a point where we would need a medium sized computer cluster to run the calculations. However, Mediavilla et al. (2017) analyzed the effects of such a bimodal distribution and concluded that even in such a case, the microlensing effects by primordial black holes would not have gone unnoticed. An alternative idea to circumvent this problem would be to analyze the microlensing magnification of the broad-line emission region, which is relatively insensitive to microlensing by small objects like stars.

An important consideration is the expected fraction of microlenses. The stellar population is responsible for a fraction in microlenses of about $\alpha = 0.2$ (Jiménez-Vicente et al. 2015a,b). On the other hand, we can expect diffuse matter like interstellar gas and dust to contribute to the total matter by about the same amount (Draine 2011). This means that PBH's can consitute to the total matter to a fraction of up to $\alpha \approx 0.6$. However, we do not know how the stellar population will play a role in our analysis, so our results might be a bit off. Anyhow, every result yielding $\alpha > 0.2$ would point towards the conclusion that we might have detected MACHOs outside of the stellar population.

4.2 The Used Code

The numerical code has undergone many changes and improvements that can not all be discussed in this thesis. Instead we will briefly present the final version and discuss the single programs. A link to the exact code can be found in the Appendix.

4.2.1 draw.py

This routine is responsible for creating the file containing all microlenses. It takes the number of lenses, the extent of the map and the parameters N_{BH} and σ as input. It then calculates the number of clusters and distributes their centers randomly. After that it assigns each microlens randomly to one cluster and computes the relative position to the cluster center. It then adds this position with the position of the cluster and checks whether the microlens is still within the map. If it is outside the map, the whole process (including the assignment to one cluster) gets repeated until the lens is within the map. The result of this method is that the size of the clusters is subject to small random fluctuations and, most importantly, that clusters that overlap with boundary regions contain appropriately less stars.

4.2.2 ipm.f

This is the IPM code developed by Mediavilla et al. (2011, 2006) in a slightly modified version. It takes the microlenses and some parameters of the macro-lens as input and calculates the magnification map, which is with the help of a small routine **pat2fits.py** saved as a fits file.

4.2.3 createhistogram.py

This routine extracts magnification histograms, one linear and one in magnitudes, out of each magnification map and afterwards deletes the map.

4.2.4 magmap.py

This script manages the creation of the magnification maps. It takes the necessary parameters (κ, γ, α, N_{BH}, σ) as input. It then creates folders for each parameter choice, compiles the **ipm.f** file, prepares the inputs and calls the IPM program. Afterwards it calls the **createhistogram.py** file and cleans up remaining files. This code is written such that multiple computers, writing to the same directory, can use it simultaneously. Also, it can call the IPM program on each computer on multiple processes, substantially increasing the number of maps generated per computer and unit time.

4.2.5 routine.py

This program handles the calling of the **magmap.py** file. Depending on the computer architecture it needs to be modified appropriately. In our case we manually enter our desired parameters, including convergence and shear, but for the use on a computer cluster it is written to read the latter two values out of a file containing a list of gravitationally lensed quasars. It then calls the main routine **magmap.py** for each set of parameters.

4.2.6 correcthistogram.py

This program is written for the analysis of the histograms. It adds all linear histograms and computes the mean magnification, which is then compared to the mean magnification of the maps to rule out errors. Afterwards it adds the histograms in magnitudes and shifts them by the appropriate amount, determined in the previous calculation.

4.2.7 bayes.py

This program performs the Bayesian analysis on the files produced by the **correcthistogram.py**-algorithm. Given two quasar images, it convolves the respective histograms and performs the Bayesian analysis, given a certain magnification range. While producing the main and final result, its workload is rather small.

4.3 The first Run

The first run was a short test to see if the code works and produces appropriate results. For this we created magnification maps for the values $\kappa = 0.4$ and $\gamma = 0.2$, yielding an average magnification of $\mu = 3.125$. While not extremely realistic for a lens system, the low magnification allows for a relatively fast computation of maps. We chose to make the map 40 Einstein radii wide with 1000 pixels in each dimension. This leads to the fact that one pixel is about 5 lightdays, so a convolution of the magnification maps is not necessary. We expect with an increased clustering of black holes more dominant features in the high magnification region but an overall tendency towards lower magnifications, while less clustered constellations should lead to a smoother histogram. We extreacted the histograms from the magnification maps and performed an autocorrelation, comparing the results for different parameters. This can be seen in Figure A.1.[10] As expected, the most prominent change arises in the modification of α. The higher the fraction of mass in microlenses, the more likely are high magnifications. There are some curious features for low values of α around ± 1.5 magnitudes, which could be attributed to noise: In the regions of smaller alpha, especially with an already small magnification, the number of microlenses is very low. As these microlenses are additionally clustered, this leads to an increased shot noise.

The other changes are more subtle: An increasing number of black holes per cluster overall seems to reduce the microlensing efficiency, however the effect is less prominent than we had hoped and expected. The image is even less clear when one considers different cluster radii. There, a turnover seems to happen, where a value of 4 Einstein radii for σ seems to favor higher magnifications with respect to 2, but the value 10 significantly disfavors higher magnifications. An example bayesian analysis was conducted for magnifications of $\Delta m = -0.3$ and $\Delta m = -0.4$. What is important is that both analyses seem to be relatively insensitive towards both cluster radius and number of black holes per cluster, but produce different results for the fraction of mass in microlenses (compare Figures 7, A.2 and A.3). We also created twodimensional plots checking for degeneracies between the parameters, an example of which can be seen in Figure A.4. Due to limited computational power and this consideration, we chose to perform the analysis of the *most likely lens* (in the next section) with α as the only variable and set $N_{\mathrm{BH}} = 300$ and $\sigma = 4$. One surprising aspect was that the mean magnification $\langle\mu\rangle$ of the maps differed from the one calculated via (5). Of course we expected some fluctuations between maps, but even after averaging many maps the mean magnification seemed off. At first we suspected an error in the code, but despite a thorough search we were unable to locate one. Then another consideration came to mind: Due to the existence of microlenses the κ in Equation (5) randomly fluctuates. By expecting that the mean magnification of the maps equals the theoretical one we implicitly assumed the equation

$$\left\langle \frac{1}{|(1-\kappa-\gamma)(1-\kappa+\gamma)|} \right\rangle = \frac{1}{|(1-\langle\kappa\rangle-\gamma)(1-\langle\kappa\rangle+\gamma)|}$$

to be true, which is generally **not** the case.

[10] All figures labeled with 'A' can be found in the Appendix.

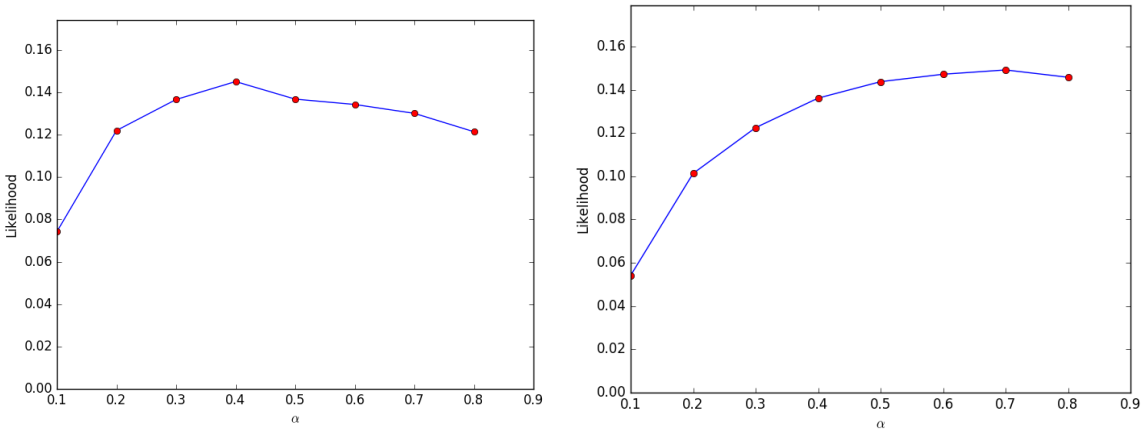

(a) $\Delta m = -0.3$ (b) $\Delta m = -0.4$

Figure 7: Comparison of the likelihoods for the fraction of mass in microlenses for a bayesian analysis with a magnification of $\Delta m = -0.3$ and $\Delta m = -0.4$.

4.4 The most likely Lens

In the next step, we consider the *most likely lens*, which has two images A and B, where A has $\gamma = \kappa = 0.45$ and B has $\gamma = \kappa = 0.55$, imposing a magnitude difference due to microlensing of $\Delta m = -0.3$. We created 100 magnification maps for each value of α, keeping the parameters σ and N_{BH} constant. As we want to compare our results to the case of unclustered black holes, we also chose to compute magnification maps for a uniform distribution of microlenses. In this case we expected to encounter significantly less shot-noise, so we chose to compute only 36 magnification maps for each value of α.

The first surprising result was the behaviour of the mean magnifications: In the case of clustered black holes the mean magnification was typically lower than the theoretical one. For $\kappa = 0.45$, $\gamma = 0.45$, an increasing parameter α yielded lower average magnifications for the clustered microlenses, dipping down to below 7. However, in the case of a uniform distribution the mean values increased with the parameter α up to about 14. In the case of $\kappa = 0.55$, $\gamma = 0.55$ the magnifications in both cases decreased with increasing α, whereas this decrease was extreme for the clustered case and barely noticeable for the uniformly distributed lenses (compare Table 2). While the dependence on α itself is understood,[11] it is still an open question as to why those values behave so differently.[12] This leads to an interesting consideration: If we use a macro model of the lens to obtain the magnification baseline of the observed quasar we will obtain the value of the theoretical mean magnification (compare Section 3.5), whereas if we use the narrow line emission region or the radio emission, we will obtain the average mean magnification of the maps as a baseline. So, depending

[11] The higher the paramter α, the lower is the contribution of the parameter κ_s (compare (6)), which is exact, to the mean magnification and the higher are the random fluctuations.

[12] A random sampling of κ in Equation (5) showed that for small fluctuations the mean magnification tends to be higher and for high fluctuations the mean magnification tends to be lower. However, the different behaviour between $(\kappa, \gamma) = (0.45, 0.45)$ and $(\kappa, \gamma) = (0.55, 0.55)$ can not be explained by this.

Table 2: Mean values of the magnification maps.

	$\kappa = 0.45, \gamma = 0.45$		$\kappa = 0.55, \gamma = 0.55$	
α	Clustered	Uniform	Clustered	Uniform
0.1	9.95	10.16	9.01	9.74
0.2	9.64	10.37	8.12	9.48
0.3	8.96	10.59	7.52	9.29
0.4	8.57	10.94	6.59	9.15
0.5	7.98	11.33	6.37	9.00
0.6	7.78	11.84	5.78	8.75
0.7	7.66	12.56	5.18	8.66
0.8	7.25	13.45	5.37	8.53
0.9	6.61	14.07	4.80	8.31
1.0	6.78	14.17	4.60	8.26

on our method to determine the magnification of the real quasar, we need to adjust our analysis of the simulations.

4.4.1 Using the mean magnification of the maps

This method should be used if one uses the radio emission or the narrow line emission region to determine the magnification of the quasar due to microlensing. We will compare the results of the clustered distribution with the ones from the uniform one. While the magnification histograms had an overall similar behaviour, they still differed significantly from one another and focused on different features. An example for this can be seen in the upper part of Figure A.5.

As one can see in the upper left part of the figure, the histogram for the clustered black holes shows a quite strong peak around a magnification of 0 magnitudes, whereas the histogram for the uniform distribution has a way lower peak at this value. Also, it is apparent that although we computed almost three times as many maps for the clustered case, the noise is still way higher. This is even more striking when one compares the single histograms, as can be seen in Figure A.6.

A comparison of the magnification histograms for different values of α can be seen in Figure 8. Here we notice that the case $\kappa = 0.45$, $\gamma = 0.45$ behaves as expected. An increase in α leads to a higher number of microlenses which in turn leads to a broadening of the magnification histogram. However, the case $\kappa = 0.55$, $\gamma = 0.55$ is another matter: First of all, the magnification histograms are way broader which is partly expected as the number of microlenses is again higher. However, in this case the general tendency seems to be that the histograms are broader for *low* values of α and get narrower with increasing α. This behaviour was unexpected. A partly explanation for that is that this image is a so called *high magnification saddle-point* image, which sometimes exerts peculiar behaviour.

Due to the fact that the saddle-point image behaves so differently, we chose to perform two Bayesian analyses: One where we cross-correlate the histograms for the values $(\kappa, \gamma) = (0.45, 0.45)$ with the ones from $(\kappa, \gamma) = (0.55, 0.55)$ (from here on reffered to as Case 1) and one which might be more representative for a 'normal' lens where we perform an auto-correlation of the histograms for $(\kappa, \gamma) = (0.45, 0.45)$ (which we will refer to as Case 2). The resulting histograms for these analyses can be found in Figure 9. A Bayesian analysis for a magnitude difference of $\Delta m = -0.3$ showed

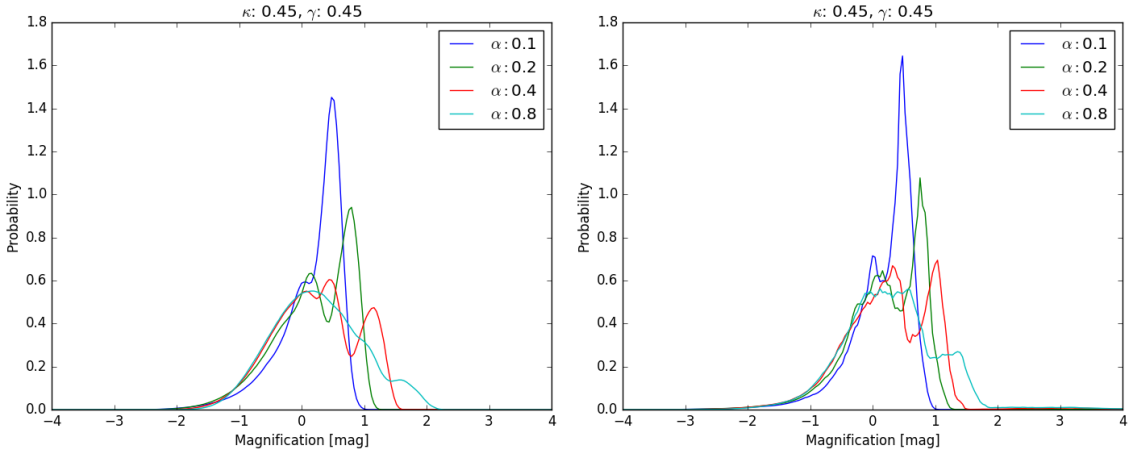

(a) Uniform Distribution

(b) Clustered Distribution

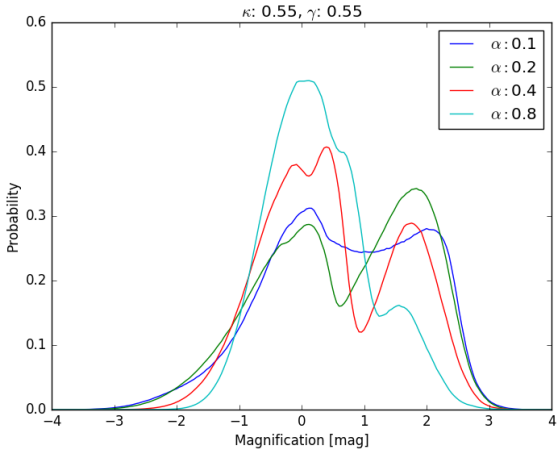

(c) Uniform Distribution

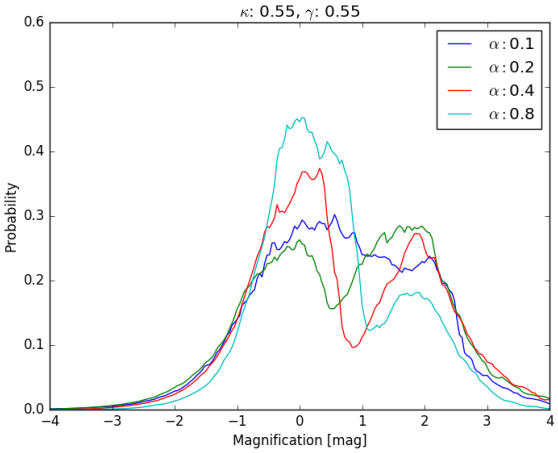

(d) Clustered Distribution

Figure 8: Magnification histograms for different values of α in the clustered and unclustered case, normalizing with respect to the mean magnification of the maps.

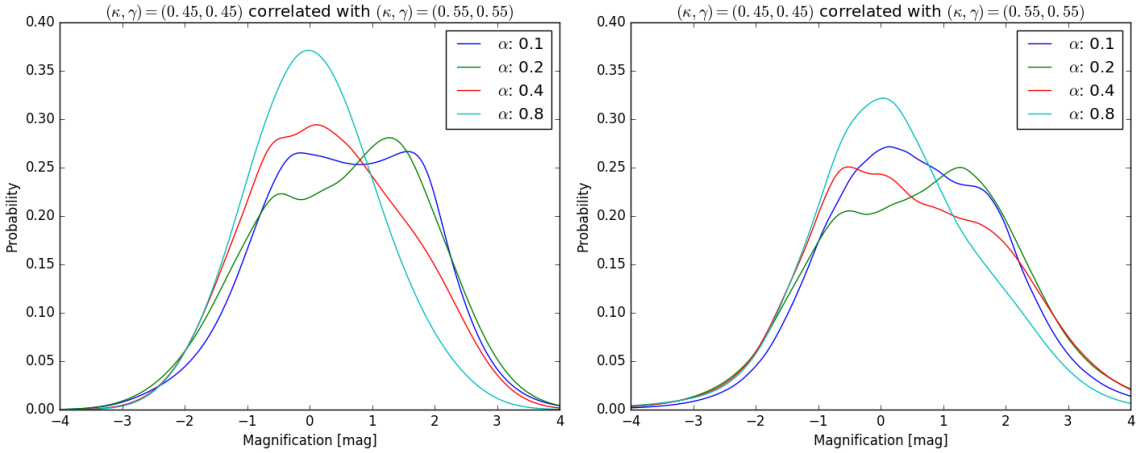

(a) Uniform Distribution, Case 1

(b) Clustered Distribution, Case 1

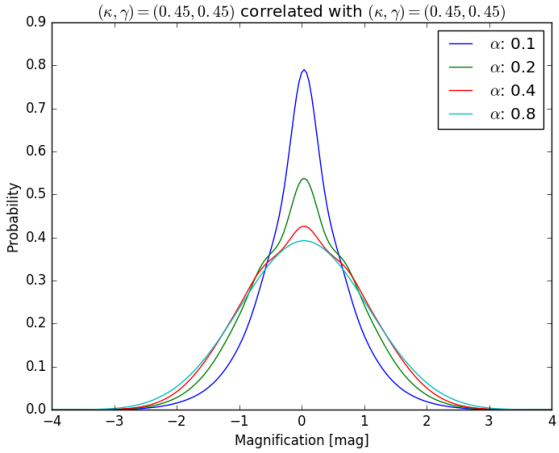

(c) Uniform Distribution, Case 2

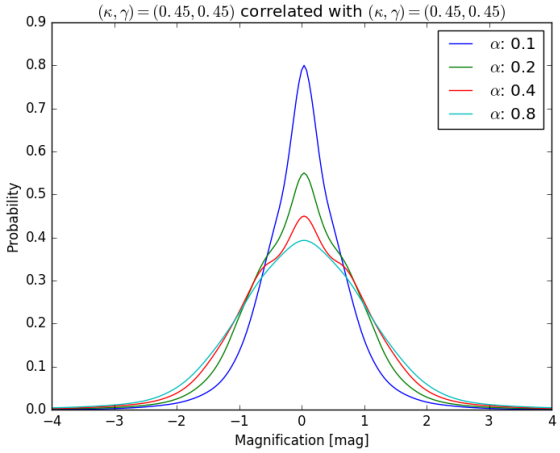

(d) Clustered Distribution, Case 2

Figure 9: Correlated histograms for different values of α in the clustered and unclustered case, normalizing with respect to the mean magnification of the maps.

that in this region the cases are fairly degenerate (compare Figure A.7). However, note that while the changes in the likelihood distribution might appear small, they become quite substantial when one analyzes a large number of quasars and multiplies their respecitive likelihood distributions.

4.4.2 Using the theoretical magnification

This method should be used when one determines the magnification of the quasar due to microlensing by a macro model of the lens. In this case we will normalize the histograms by the theoretical mean value obtained from the parameters κ and γ. The change from a magnification of 7 to 10 resp. from 14 to 10 are responsible for a shift in the histograms of about 0.35 magnitudes. As one can see in Figure A.5, for low values of α the different shift of the histograms is barely noticeable, but for high values of α the appearence differs significantly.

We performed an analogous analysis as in the previos section. Inspecting Figure A.8 we see that in contrast to Figure 8 especially the histograms corresponding to higher fractions of mass in microlenses are noticeably shifted. The correlated histograms also exhibit a slightly differnt behaviour (compare Figure A.9 with Figure 9), although in the overall picture they look fairly similar. However, a bayesian analysis with magnitude difference $\Delta m = -0.3$ does indeed yield a different result (compare Figures A.10 and A.7).

5 Discussion

Due to the huge amount of computation time needed to construct the magnification maps (and the huge amount of maps needed due to shot-noise) we were yet unable to perform an analysis based on real data. We need to perform these calculations, times 9 (to include the variables N_{BH} and σ), for about 30 observed quasars. With that in mind, answering the question 'Is the existence of primordial black holes consistent with the data from quasar gravitational microlensing?' based on this thesis is impossible. Within the next weeks we will be able to run the code on a computer cluster and with the resulting data we will be able to find an answer. For this thesis, the question reads: 'Do the results of Mediavilla et al. (2017) exclude the existence of clustered primordial black holes?' and to this we can answer: Maybe not.

We have seen that in general the probability distribution of magnifications for clustered lenses behaves roughly like the one for unclustered ones. The general features (broadening of the distribution with different α's, number of peaks in the histogram, ...) are mostly the same, however the histograms still differ by a significant amount: Sometimes the location or height of the peaks change and one can observe that the histograms for clustered lenses are in general broader. For some lens systems (i.e. Case 2) the correlated probability distributions are, albeit a bit broader in the clustered case, almost the same. However, for other lenses (i.e. Case 1) the correlated probability distributions exhibit very different behaviour (compare Figure 9). Our bayesian analysis was conducted in a region where the histograms are quite similar, but it is not unlikely that the analysis of the real lenses will include the study of those regions that differ between the clustered and unclustered case.

Also, we can conclude that one has to pay close attention to the method which is used for the determination of the quasar magnification baseline. The differences in the mean magnification between a clustered and a uniform distribution of microlenses are fairly substantial and may have a significant impact on the results of the analysis. The fact that the average magnification in the

clustered case was so much lower shows that, as expected, clustered lenses seem to be less efficient in microlensing, compared to a uniform distribution.

We are of course far from giving a definite answer to the question, but we have shown that there are indeed subtle differences between the behaviour of clustered and uniformly distributed lenses. It is now up to the oncoming analysis to show whether these differences are significant enough to explain gravitational microlensing data under the premise of the existence of primordial black holes.

A study involving this many assumptions is naturally prone to systematic errors, of which we have already discussed a few in the thesis:

- The radial profile of a cluster of primordial black holes is probably not a Gaussian one. More suitable candidates might be some truncated form of the singular isothermal sphere, for example a King profile often used in the analysis of star clusters (King 1962). However, trading our one-parameter profile for a two- or even three-parameter profile does not seem like a good idea considering our already large parameter space. We believe that among all systematic errors, the contribution of the radial profile is not significant as in our group we have performed a comparison with a uniform radial profile and found no significant differences in the resulting histograms.

- We are considering a source size of 5 lightdays for the continuum emission region. This source size is consistent with results from reverbration mapping, which is independent from gravitational microlensing thus avoiding circularity of our model. However, subtle changes in the size of the source might still have an impact on our results.

- We are neglecting the stellar population and the clustering efficiency of the black holes. Both are physically very motivated: Obviously a stellar population in galaxies exists and the fact that not all stars and galaxies are bound in clusters gives rise to the assumption that the same would hold for primordial black holes. However, both of these aspects would increase our computational time again by a large amount (one by adding an additional paraemter, the other by multiplying the number of microlenses by about 100) and Mediavilla et al. (2017) showed that even neglecting these effects the existence of primordial black holes would lead to a result inconsistent with the values for the current stellar population.

- We have just considered clusters of a constant size (albeit with some random fluctuations). As microlensing is fairly insensitive to the slope of the mass spectrum of the lenses, one might be tempted to assume that similarly it is just sensitive to the average size of the clusters and not to the distribution of their sizes. However, to our knowledge this has not yet been studied.

- We have already discussed the different methods of determining a baseline for the quasar magnification, each of which is prone to its own systematic errors (extinction, uncertainties in the macro model, magnification of the narrow line emission region due to the huge caustics introduced by the clusters). We have also discussed that depending on the method of baseline-determination, a different analysis has to be performed.

- As in all studies involving the nature of Dark Matter we face a certain circularity. The unterlying ΛCDM model we use to calculate distances (which is essential for our study) already uses assumptions about Dark Matter. Unfortunately there is no satisfying way to avoid this problem.

All things considered, we are relatively confident that the systematic uncertainties are less important than factors like the shot noise of the magnification maps and the limited number of quasar images available for study (especially since the determination of the baseline is more difficult in this case). However, if we were to be able to increase our computational resources, we would probably include a background stellar population and a variable factor for the clustering efficiency.

6 Conclusion

During this thesis we have created a python script that can be used to build magnification maps for a clustered distribution of lenses, extract the probability distribution functions, normalize them with respect to the mean magnification and perform a cross-correlation including a following bayesian analysis. This code has been used on a small laptop, on a computer farm and on a large computer cluster. It can be run on every system that has python (and a few submodules) installed and uses the GNU fortran compiler (although using another fortran compiler would just require the change of one line of code). The initial values (κ, γ) can be either entered manually or taken from a *lens.dat* file. The values for the parameters can also be changed if one prefers another set. Everything except the creation of magnification maps and the extraction of the respective histograms (which should be done on a computer farm or cluster) can be handled by a small laptop in a matter of seconds.

We used this code to perform a short test run and a case-study for the most likely lens, finding that, although the results are fairly similar to the ones based on a uniform, unclustered distribution of lenses, there are subtle differences that might make an impact in further analysis. Especially we found that clustered lenses appear to be generally less efficient in microlensing, although the effects are dependent on the chosen κ and γ. Due to this consideration we found that one has to perform a different analysis depending on which method was used to determine the magnification baseline of the lensed quasar.

A Appendix

A.1 Additional Figures

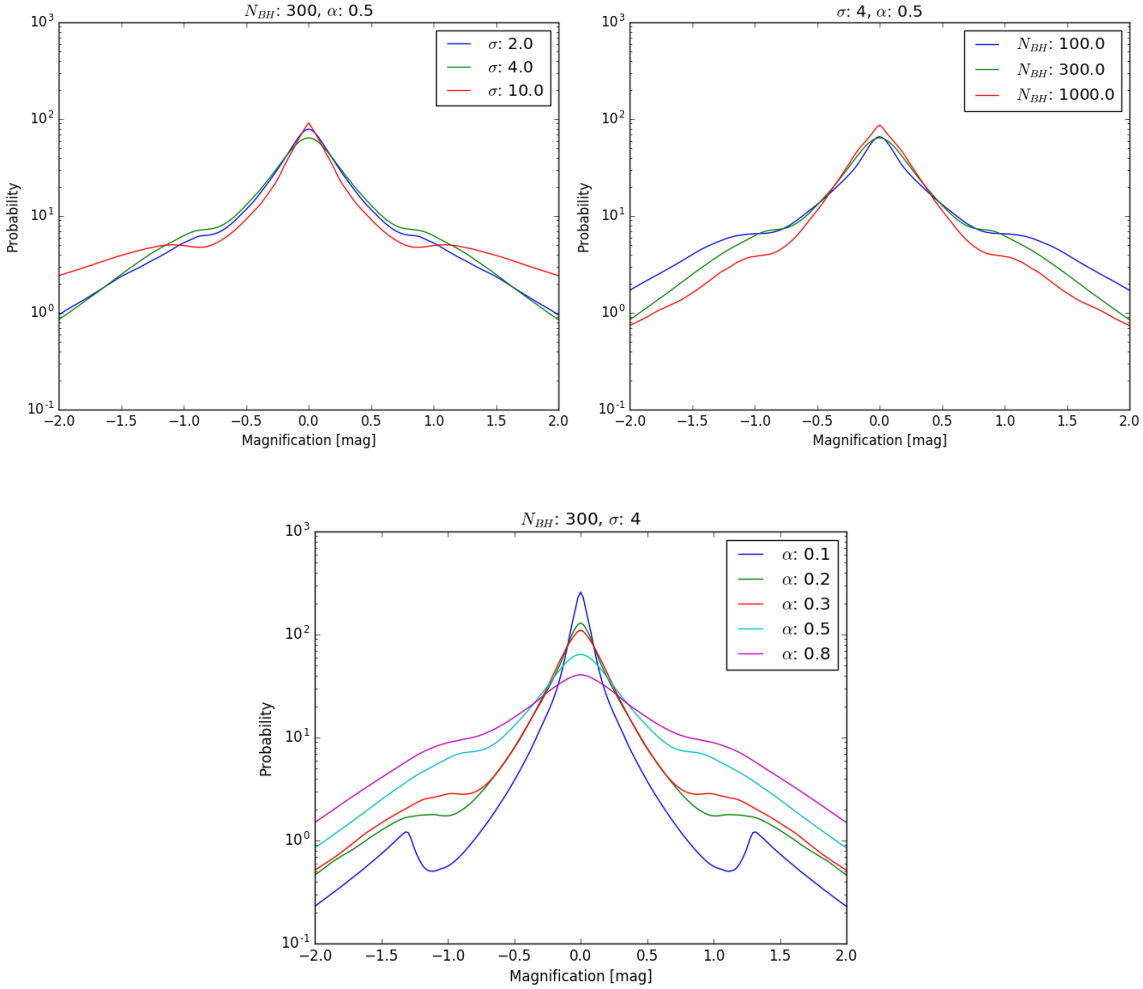

Figure A.1: Comparison of the autocorrelated histograms for different parameter choices.

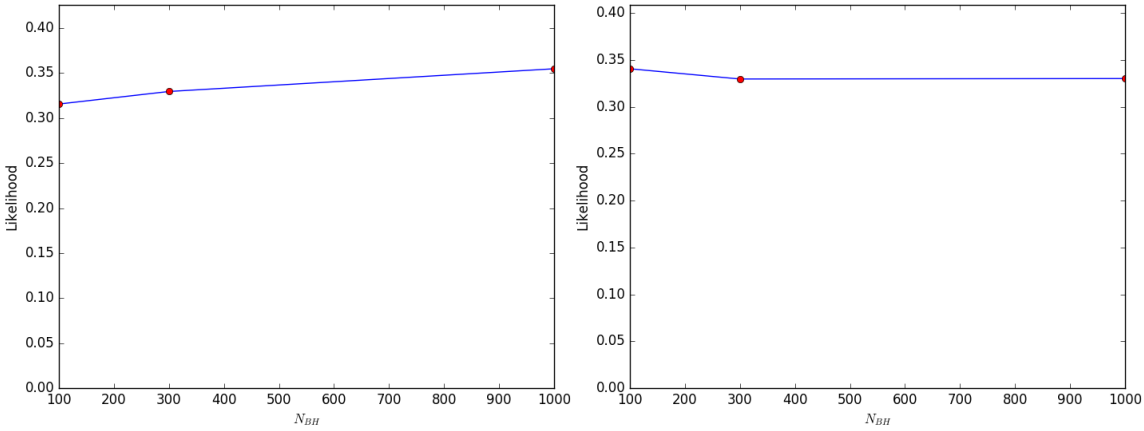

(a) $\Delta m = 0.25$ (b) $\Delta m = 0.4$

Figure A.2: Comparison of the Likelihoods for the number of black holes per cluster for a bayesian analysis with a magnification of $\Delta m = 0.25$ and $\Delta m = 0.4$.

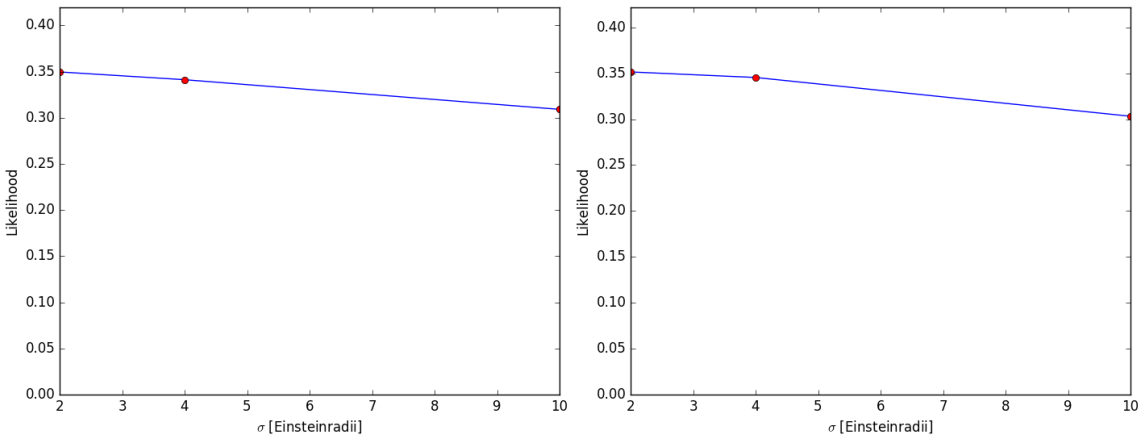

(a) $\Delta m = 0.25$ (b) $\Delta m = 0.4$

Figure A.3: Comparison of the Likelihoods for the extent of the clusters for a bayesian analysis with a magnification of $\Delta m = 0.25$ and $\Delta m = 0.4$.

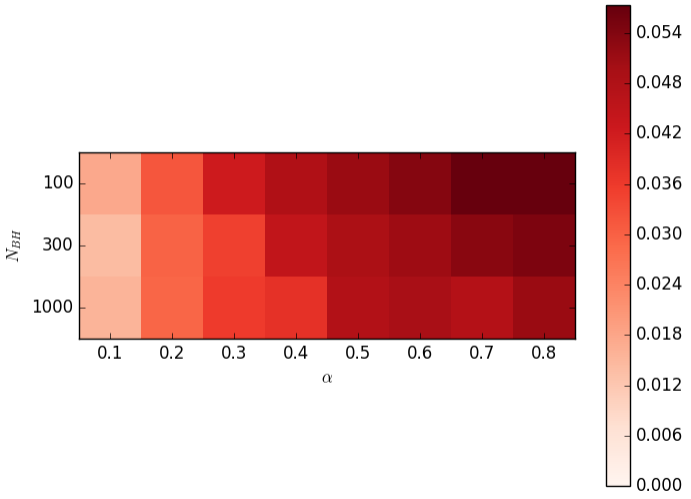

Figure A.4: Example of a twodimensional likelihood distribution between the parameters N_{BH} and α in a bayesian analysis with $\Delta m = -0.4$.

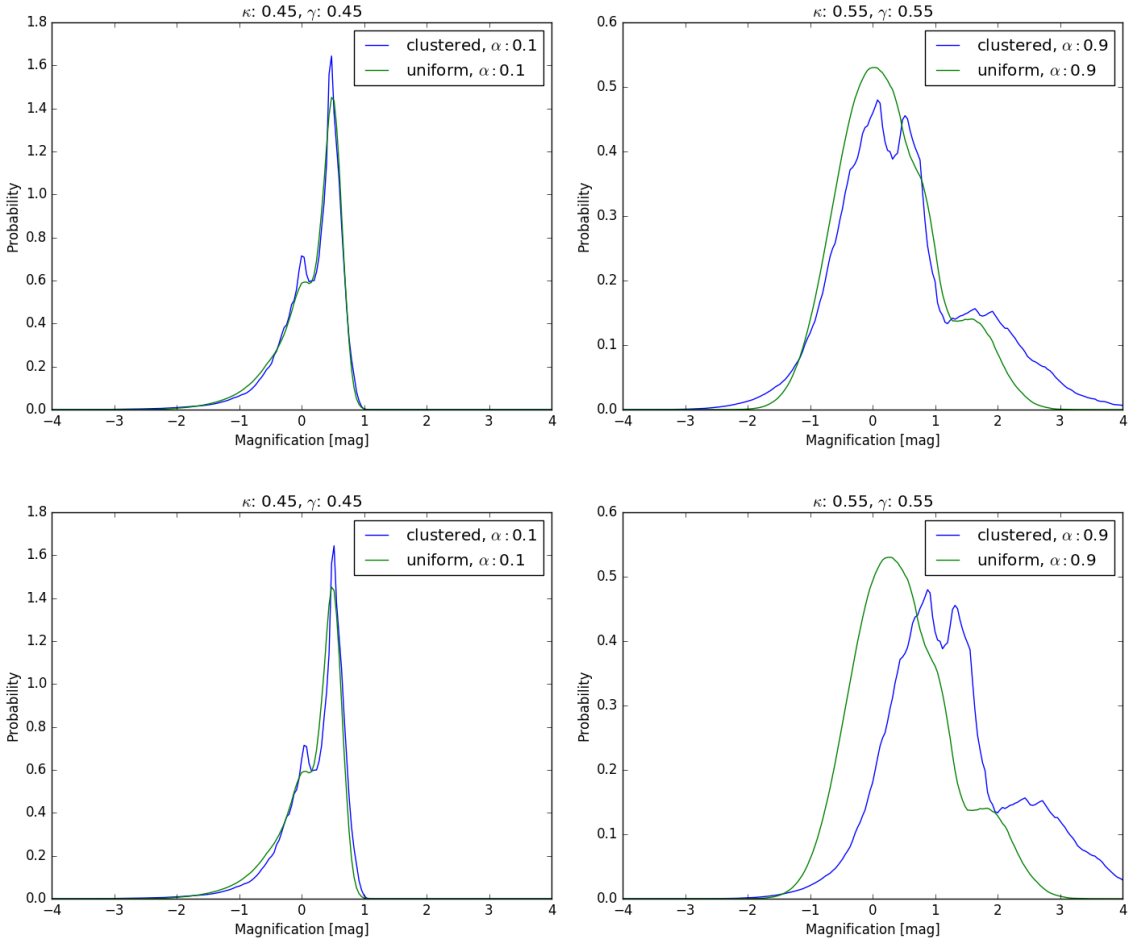

Figure A.5: Two examples for magnification histograms comparing the clustered and unclustered case. The upper ones are normalized with respect to the mean magnification of the maps, whereas the lower ones are normalized with respect to the theoretical mean magnification.

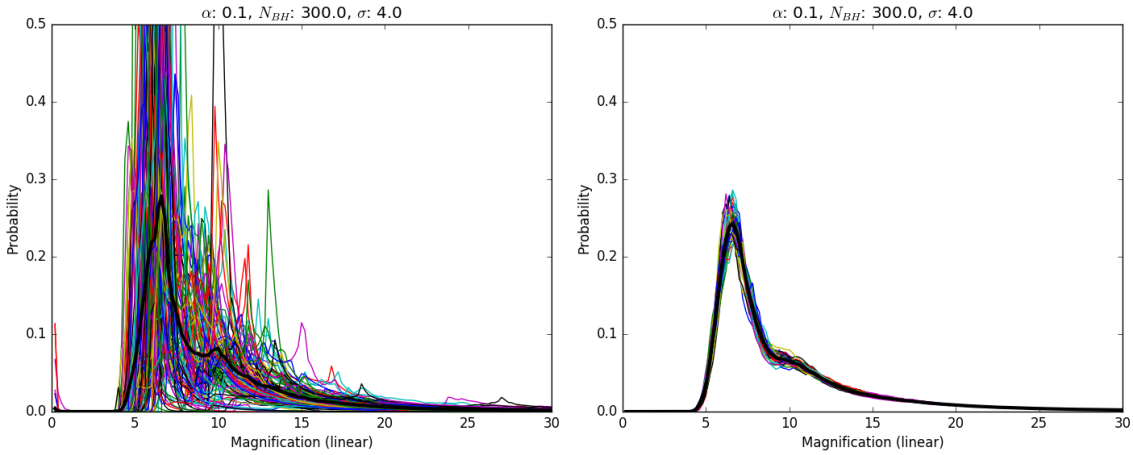

(a) Clustered Distribution (b) Uniform Distribution

Figure A.6: Two examples for magnification histograms comparing the clustered and unclustered case. The colored lines correspond to the single histograms extracted from each map, the thick black line represents the average.

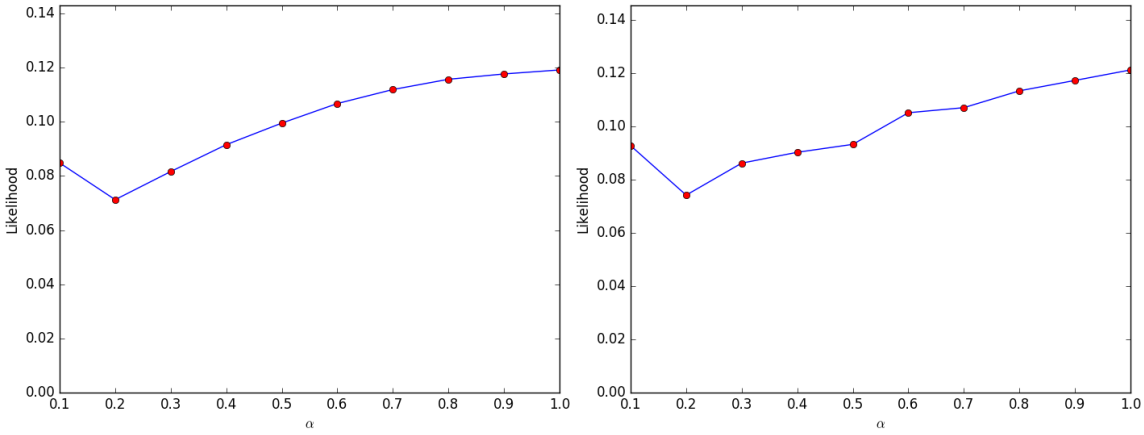

(a) Uniform Distribution, Case 1

(b) Clustered Distribution, Case 1

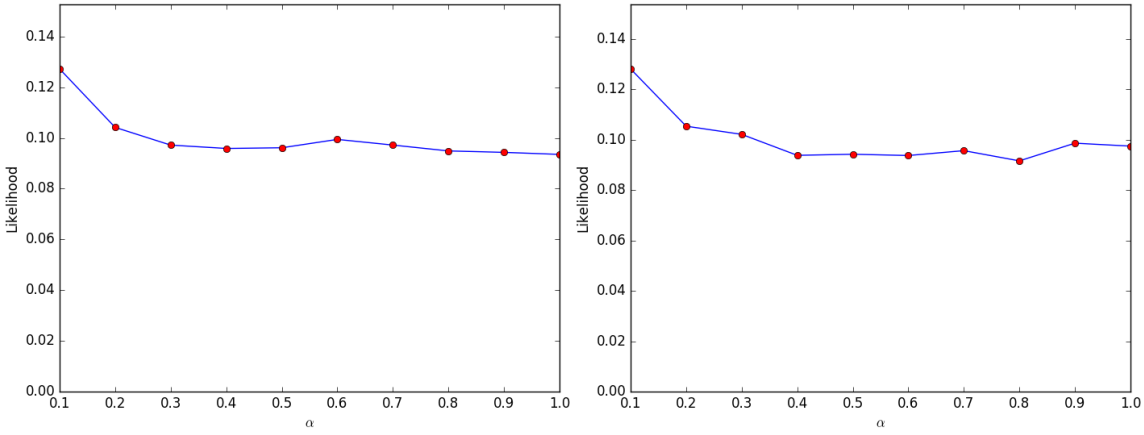

(c) Uniform Distribution, Case 2

(d) Clustered Distribution, Case 2

Figure A.7: Results of the bayesian analysis for a magnitude difference of $\Delta m = -0.3$, normalizing with respect to the mean magnification of the maps.

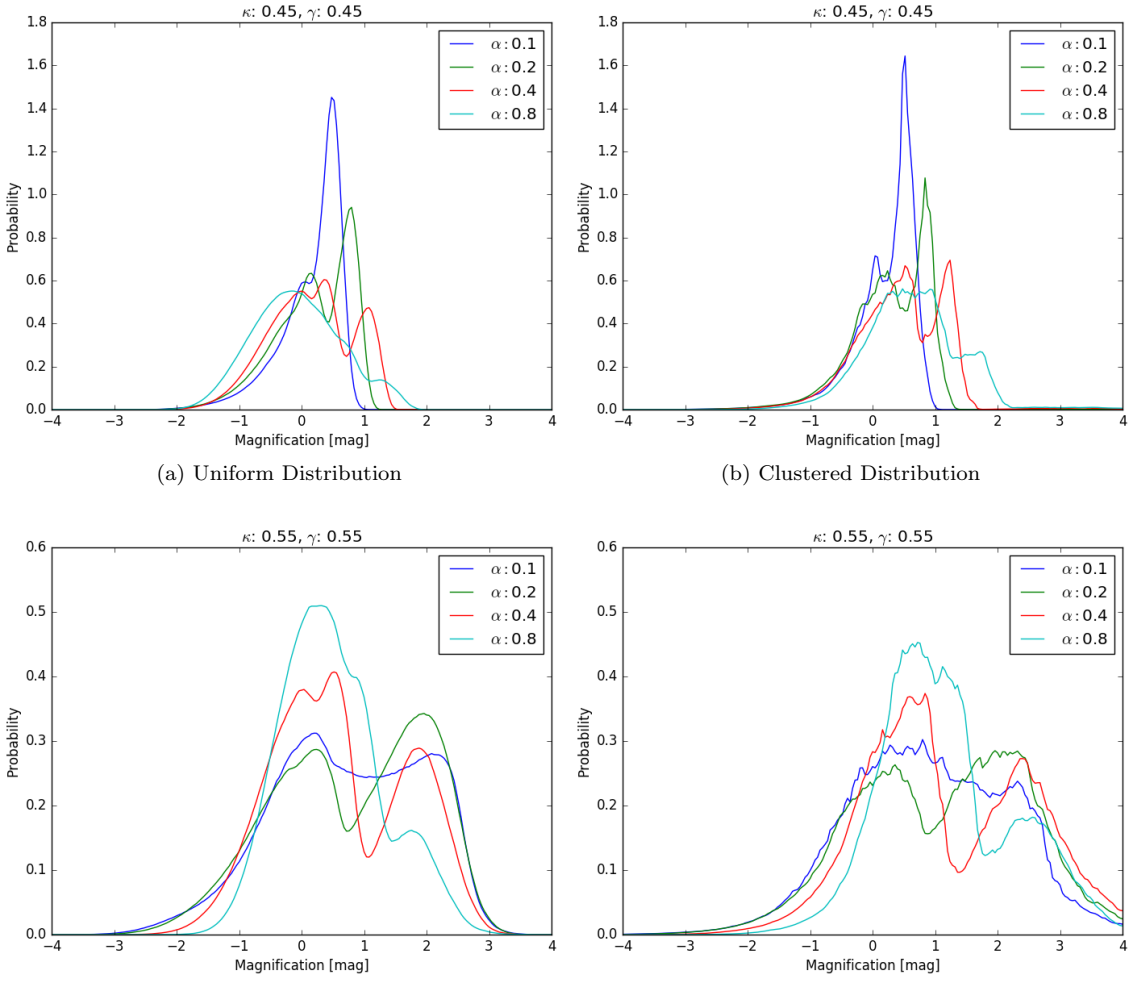

(a) Uniform Distribution

(b) Clustered Distribution

(c) Uniform Distribution

(d) Clustered Distribution

Figure A.8: Magnification histograms for different values of α in the clustered and unclustered case, normalizing with respect to the theoretical mean.

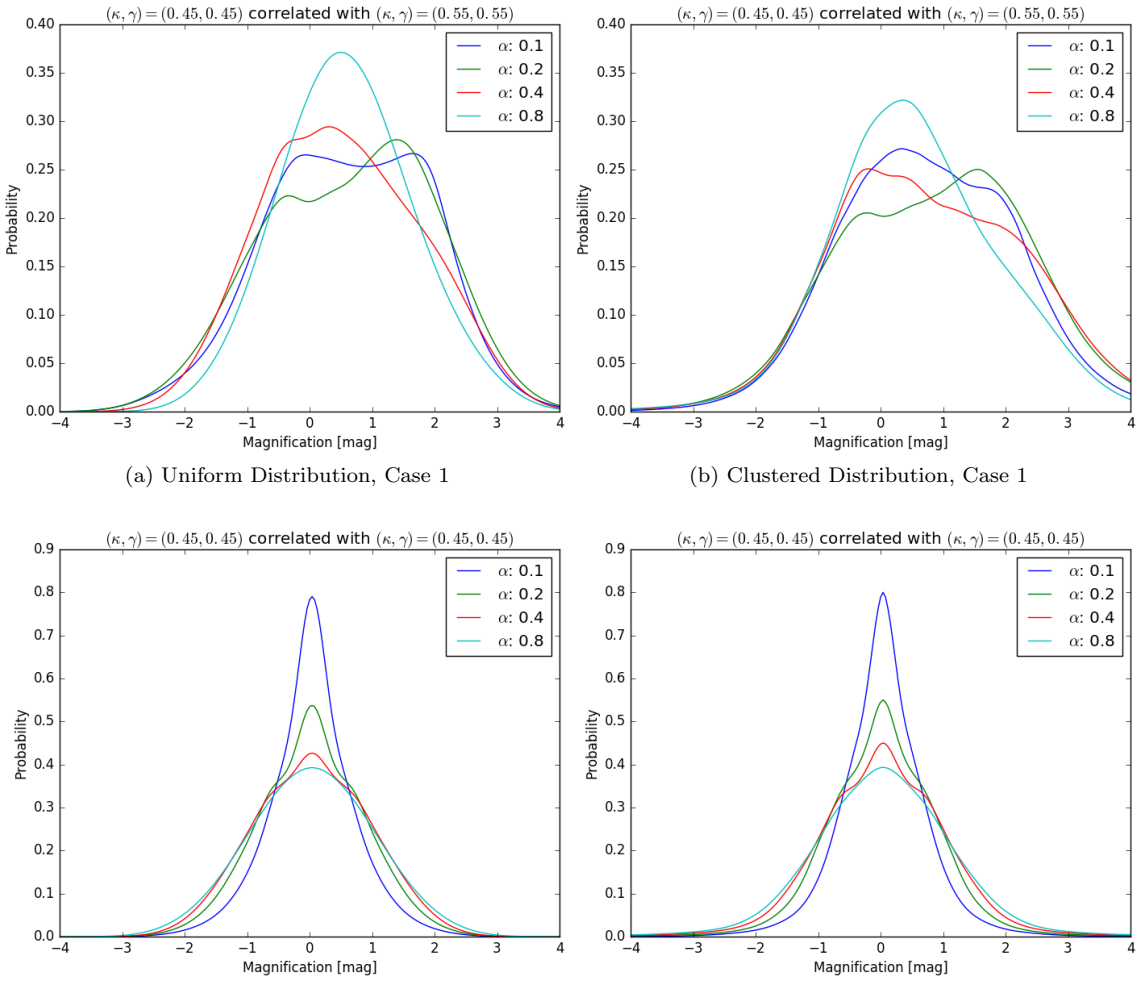

(a) Uniform Distribution, Case 1

(b) Clustered Distribution, Case 1

(c) Uniform Distribution, Case 2

(d) Clustered Distribution, Case 2

Figure A.9: Correlated histograms for different values of α in the clustered and unclustered case, normalizing with respect to the theoretical mean.

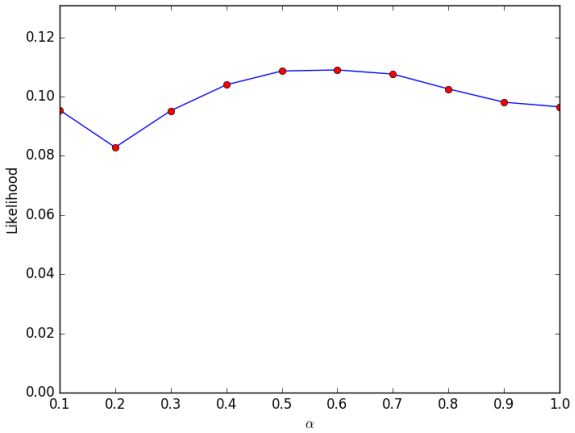

(a) Uniform Distribution, Case 1

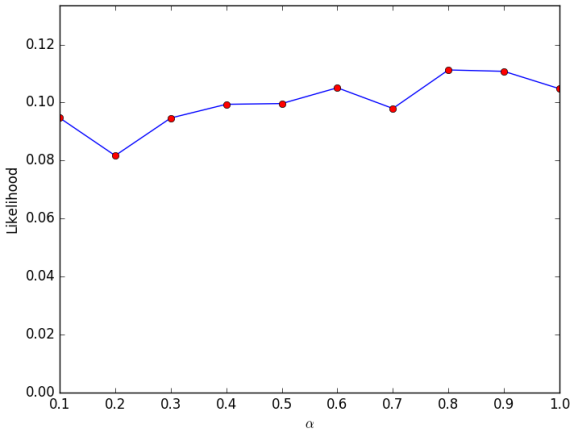

(b) Clustered Distribution, Case 1

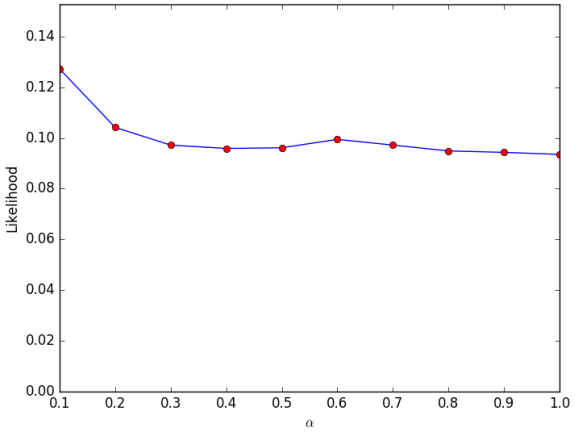

(c) Uniform Distribution, Case 2

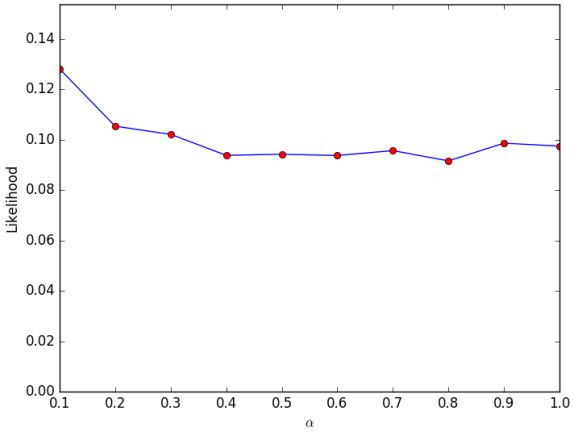

(d) Clustered Distribution, Case 2

Figure A.10: Results of the bayesian analysis for a magnitude difference of $\Delta m = -0.3$, normalizing with respect to the theoretical mean.

A.2 The used code

Below the reader can see a short example for the 'routine.py' module which is used to run the code on the computer farm. All in all, over 1300 lines of code were written, which can not all be displayed here. All files used for the creation and analysis of the magnification maps can be found in the google drive: https://goo.gl/nRqG2h

```
import subprocess
import os

alphas = [0.0625,0.125,0.25,0.5,0.75,1.0]
radii = [1,2,4]
concentrations = [100,300,1000]
numruns = 25

data = open('lenses.dat','r')
lenses = data.readlines()
data.close()
nl=0
for lens in lenses:
    [name,kappa,gamma,dl,ds,dls] = lens.split()
    nl=nl+1
    for alpha in alphas:
        for radius in radii:
            for concentration in concentrations:
                alpha = str(alpha)
                radius = str(radius)
                concentration = str(concentration)
                for j in range(numruns):
                    command = ['python3', 'magmaps.py', name, alpha, concentration, radius,
                        kappa, gamma, str(j)]
                    subprocess.call(command)
```

List of Figures

List of Tables

References

Abbott, B. P., Abbott, R., Abbott, T. D., et al. 2016a, Physical Review Letters, 116, 241103

Abbott, B. P., Abbott, R., Abbott, T. D., et al. 2016b, Physical Review Letters, 116, 061102

Abbott, B. P., Abbott, R., Abbott, T. D., et al. 2017a, Physical Review Letters, 118, 221101

Abbott, B. P., Abbott, R., Abbott, T. D., et al. 2017b, ApJ, 851, L35

Abbott, B. P., Abbott, R., Abbott, T. D., et al. 2017c, Physical Review Letters, 119, 141101

Becker, A. C., Alcock, C., Allsman, R. A., et al. 1999, in Bulletin of the American Astronomical Society, Vol. 31, American Astronomical Society Meeting Abstracts, 1444

Bennert, N., Falcke, H., Schulz, H., Wilson, A. S., & Wills, B. J. 2002, ApJ, 574, L105

Cao, L., Lu, Y., & Zhao, Y. 2018, MNRAS, 474, 4997

Carr, B., Kühnel, F., & Sandstad, M. 2016, Phys. Rev. D, 94, 083504

Chang, K. & Refsdal, S. 1979, Nature, 282, 561

Chen, Z.-F., Qin, Y.-P., Chen, Z.-Y., & Lü, L.-Z. 2011, Journal of Astrophysics and Astronomy, 32, 273

Clesse, S. & García-Bellido, J. 2017a, Physics of the Dark Universe, 18, 105

Clesse, S. & García-Bellido, J. 2017b, ArXiv e-prints [arXiv:1711.10458]

Congdon, A. B., Keeton, C. R., & Osmer, S. J. 2007, MNRAS, 376, 263

Dai, L., Venumadhav, T., & Sigurdson, K. 2017, Phys. Rev. D, 95, 044011

DAMPE Collaboration, Ambrosi, G., An, Q., et al. 2017, Nature, 552, 63

Draine, B. T. 2011, Physics of the Interstellar and Intergalactic Medium

Elbert, O. D., Bullock, J. S., & Kaplinghat, M. 2018, MNRAS, 473, 1186

Ezquiaga, J. M., Garcia-Bellido, J., & Ruiz Morales, E. 2017, ArXiv e-prints [arXiv:1705.04861]

Fausnaugh, M. M., Denney, K. D., Barth, A. J., et al. 2016, ApJ, 821, 56

García-Bellido, J. 2017, in Journal of Physics Conference Series, Vol. 840, Journal of Physics Conference Series, 012032

García-Bellido, J. & Clesse, S. 2017, ArXiv e-prints [arXiv:1710.04694]

Jiménez-Vicente, J., Mediavilla, E., Kochanek, C. S., & Muñoz, J. A. 2015a, ApJ, 799, 149

Jiménez-Vicente, J., Mediavilla, E., Kochanek, C. S., & Muñoz, J. A. 2015b, ApJ, 806, 251

King, I. 1962, AJ, 67, 471

Mediavilla, E., Jiménez-Vicente, J., Muñoz, J. A., Vives-Arias, H., & Calderón-Infante, J. 2017, ApJ, 836, L18

Mediavilla, E., Mediavilla, T., Muñoz, J. A., et al. 2011, ApJ, 741, 42

Mediavilla, E., Muñoz, J. A., Falco, E., et al. 2009, ApJ, 706, 1451

Mediavilla, E., Muñoz, J. A., Garzón, F., & Mahoney, T. J. 2016, Astrophysical Applications of Gravitational Lensing

Mediavilla, E., Muñoz, J. A., Lopez, P., et al. 2006, ApJ, 653, 942

Meylan, G., Jetzer, P., North, P., et al., eds. 2006, Gravitational Lensing: Strong, Weak and Micro

Mortonson, M. J., Schechter, P. L., & Wambsganss, J. 2005, ApJ, 628, 594

Mosquera, A. M. & Kochanek, C. S. 2011, ApJ, 738, 96

Nakama, T., Carr, B., & Silk, J. 2017, ArXiv e-prints [arXiv:1710.06945]

Navarro, J. F., Frenk, C. S., & White, S. D. M. 1996, ApJ, 462, 563

Navarro, J. F., Frenk, C. S., & White, S. D. M. 1997, ApJ, 490, 493

Planck Collaboration, Ade, P. A. R., Aghanim, N., et al. 2016, A&A, 594, A13

Poulin, V., Serpico, P. D., Calore, F., Clesse, S., & Kohri, K. 2017, Phys. Rev. D, 96, 083524

Schneider, P. 2015, Extragalactic Astronomy and Cosmology: An Introduction

Schneider, P. & Weiss, A. 1987a, A&A, 171, 49

Schneider, P. & Weiss, A. 1987b, Max Planck Institut fur Astrophysik Report, 311

Smith, G. P., Jauzac, M., Veitch, J., et al. 2017, ArXiv e-prints [arXiv:1707.03412]

Yonehara, A. 2006, ApJ, 646, 16

Zwicky, F. 1933, Helvetica Physica Acta, 6, 110

Statutory Declaration

I hereby affirm that I have carried out this work without using any other means than those indicated. All passages taken verbally or analogously from published and unpublished writings are marked as such. The work has not yet been submitted in the same or similar form or excerpts from another examination.

San Christobal de La Laguna, January 21, 2018,